A Wireless Charging Solution for the Zebro

Bachelor thesis

Richard Coesoij (4318765)
Jelmer van der Hoeven (4302281)

Technische Universiteit Delft

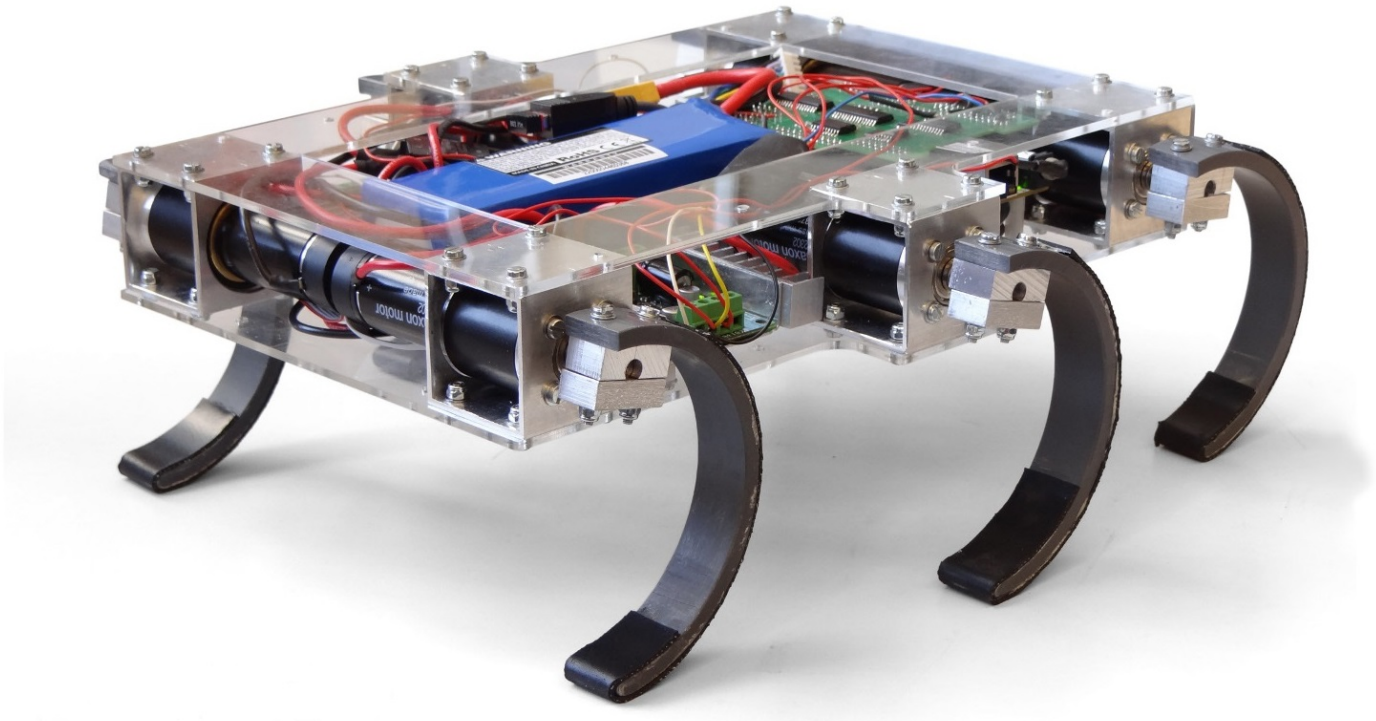

TU Delft Delft University of Technology

Challenge the future

Abstract

The Zebro is a six legged autonomous robot, designed to be deployed in swarms. Charging the battery is still done manually. To further increase the autonomous abilities of the Zebro, a wireless charging station and module is designed. The charging station is fully modular and interconnected by charging pads. This opens the possibility of charging multiple Zebro's simultaneously. The charging module consists of a receiver and Battery Management System inside the Zebro.

In this thesis, both the transmitter and receiver side of the Wireless Power Transfer (WPT) system is designed. The transmitter and receiver must be perfectly aligned for high efficiency in a wireless charging setup. The positioning of the Zebro is not highly accurate, therefore the design of an inductive WPT system using SS-topology compensation is presented. Also, possible solutions improving the efficiency of the power transfer and the WPT system is proposed in this thesis. These improvements include coil optimization, object detection, circuit damage protection and implementation into the overall system.

Preface

This thesis is part of the Bachelor Graduation Project for the bachelor in Electrical Engineering at the faculty EEMCS of the Technical University of Delft. The ZEBRO team is the proposer of this thesis. The subject of the proposal is: Research and development of an autonomous charger module and charging station for Deci Zebro. This thesis describes the wireless power transfer necessary for the charging module.

Our thesis would not have been possible without the guidance and assistance of several people. We would like to thank the following people:

The ZEBRO team
Ronald Bos
Edwin Hakkennes
Daniël Booms
Chris Verhoeven

Richard Coesoij
Jelmer van der Hoeven
Delft, 19 june 2017

Contents

1

Introduction

The ZEBRO project is an initiative of the TU Delft to research swarm-related behaviour of simple and straight-forward robots (ZEBRO's). The purpose of a ZEBRO is to cooperate with its colleagues to perform tasks which are not suitable for bigger robots and would be time consuming for humans. An example of such a task is the mapping of a disaster area.

The ZEBRO's come in different sizes. The emphasis of the design for autonomous charging will be laid on the deci-ZEBRO, where an expansion to the kilo-ZEBRO may be possible.

The ZEBRO's are completely autonomous robots. In the current design state, the battery has to be manually disconnected, recharged, and reconnected. This defeats the purpose of the autonomous behaviour of the robot. A goal set by the ZEBRO team is to have a swarm of 100 robots by the end of June 2017. In such an expanded swarm, the manual connection method is very time consuming. For this reason, an autonomous charging station and charger module are needed.

The global charging scheme is as follows. The charger module will sense when the battery is running low, and send a signal to the top-level that the ZEBRO needs to recharge. The ZEBRO will then check if there is a charging station nearby and if there is a charging spot available. If so, the ZEBRO can go to this charging station where the charging will be done autonomously. Being fully charged, the ZEBRO can continue with its tasks.

The design of the charging station and the charging module can be split up in three sub components. First, the charging station itself, converting power from a wall socket to the ideal voltage to transfer by means of inductance. The second component is about transferring the received power. The final sub component is the internal battery management system in the ZEBRO. An overview of the whole charging system is shown in fig. 1.1 The emphasis of this particular thesis is laid on the design of a wireless power transfer (WPT) system.

Wireless charging has its advantages when compared with wired charging. These advantages include, spatial freedom and preventing bad connections which could result in high losses. However, wireless power transfer introduces a new set of problems. The challenges regarding the WPT system can be split up in multiple parts.

Firstly, efficiency of the wireless system has to be optimized. For the wireless system as a whole, it competes with the wired solution with similar efficiencies [1]. For the whole system a high efficiency can be achieved when all the parts of the system are designed optimally. In the scope of this project this can not be achieved. However, a decision is made in the following sections which part of the system can be improved for the given application.

Secondly, the vertical distance and horizontal misalignment cause a less efficient power transfer. Vertical distance is to be optimized by minimizing the distance between the robot and the charging pad.

Horizontal misalignment is a bigger issue since the robot has to align itself perfectly for optimal power transfer. State-of-the-art technology offers solutions for this problem.

Thirdly, detecting a robot and switching from standby mode to active mode has to be achieved to guarantee safety of the system. This part also includes feedback theory. Also, over voltage and current protections of the system have to be implemented to guarantee the safety of the system.

Thesis structure

The design requirements of the system are described in chapter 2. This is followed by the theory behind WPT and is discussed in chapter 3, this chapter also deals with the safety standard and state of the art. After the design requirements are stated, the design is explained in chapter 4. Prototypes were build and tested to verify the design choices, this is documented in chapter 5. The final chapter, chapter 6, is a conclusion of the whole project, the test results and the design process, it also contains possible improvements.

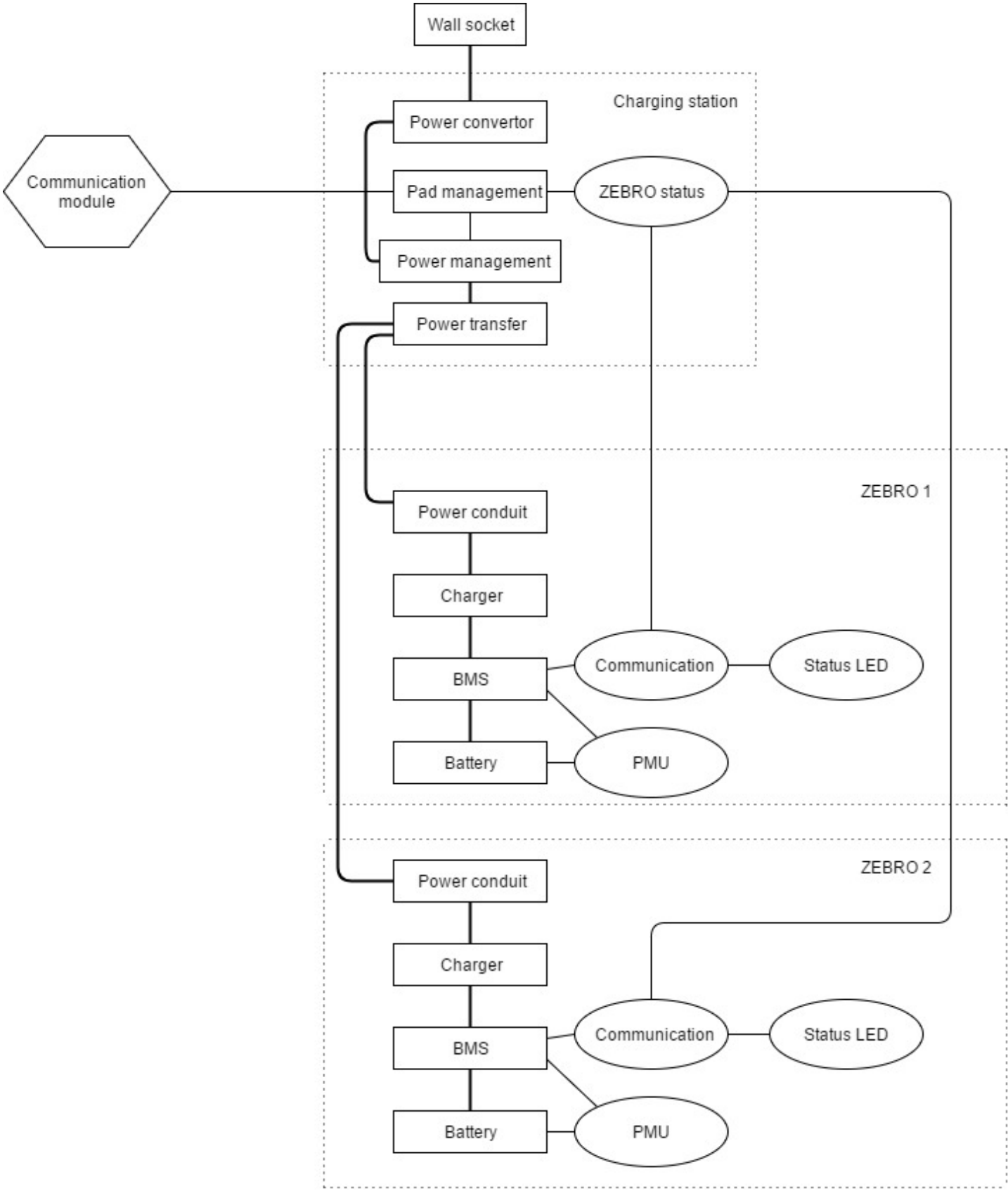

Figure 1.1: Overview of the whole system

2

Design requirements

The WPT system is designed for the ZEBRO robot. In this section, design restrictions and requirements are formulated. Restrictions and requirements include the physical dimensions of the robot, protection of the circuits and legal safety measures. The system can be split into several parts. This section starts with general requirements given by the Zebro team. Then requirements are given for the interfaces. The interface is defined as the connection to the charging pad and the Battery Management System (BMS) of the robot. Then requirements are set for the primary and secondary side located inside the charging pad and on the ZEBRO, respectively. Lastly, an overview is given in table 2.1 of the complete system.

2.1. General requirements

The ZEBRO team formulated general requirements for the charging station and module. An overview will be presented in this section.

- Charging Station Requirements
    1. The system should be expandable for multiple ZEBRO's
    2. The system should charge wireless using the QI standard
    3. Charge ZEBRO within 15 minutes
    4. Well-defined interface to the outside world
- Charging Module Requirements
    1. The module should be self-contained
    2. Charge 2 ZEBRO's using the QI standard
    3. Damage Protection System
    4. Measure current and power flow, internal temperature, alignment to station.

2.2. System requirements

Physical dimensions pose restrictions on the overall system. The charging pad is chosen to be a square with sides of 27cm. This is equal to the length of the ZEBRO robot. The thickness of the pad depends on the hardware that will be implemented and as of yet unknown. The ZEBRO robot physical dimensions can be found in the ZEBRO Git.

To make sure the WPT system and the rest of the charging system work together, agreements are made on the interfaces of the WPT. The WPT is situated at the core of the charging system. Therefore, the input and output voltage has been agreed upon. For an input voltage 48 volts has been chosen and for the output a range from 6-32 volts. This design choice will be discussed in the design section.

Furthermore, to charge the battery within a certain amount of time the system has to deliver enough power. The amount of time to fully charge is chosen to be approximately 30 minutes. This is specified by the battery management group. Because of this requirement a 100W power transfer is needed, for the battery that is to be used. This will also be the maximum power since 100 percent efficiency can not be guaranteed.

Prior to designing the operational frequency (ω_0) of the system, an agreement has been made on the range of ω_0. Since the ω_0 of the power transfer could interfere with the $\omega_{0_{BMS}}$ of the BMS, the agreement has been made that the ω_0 of the WPT should be in the order of 10^5 Hz. The BMS will operate at a frequency ten times higher.

2.2.1. Primary side

System requirements for the primary side are the following:

- Input DC voltage of 48 volts
- Overcurrent protection
- Optimizing power transfer
- Detecting the ZEBRO robot or detecting a foreign object (FOD)

Over-current protection has to be in place at the primary side, in case that the current through the primary coil will be too high. A high current through the coil causes a magnetic field that could damage the electronics or harm the environment. Also, the circuitry near the magnetic field will be affected. The maximum current through the primary coil is set to be 2.5 amperes.

Next, the primary side has to determine whether a robot is to be charged or not. This requirement is needed such that no power will be lost. Also, this detection method can determine whether or not a foreign object is placed on the charging station. Will this be the case, high temperatures could occur, which would damage the system.

2.2.2. Secondary side

System requirements for the secondary side are the following:

- DC output, with a maximum ripple 0.5V
- Output voltage between 6V and 32V
- Over-voltage protection
- Optimizing power transfer to load
- Dimension of PCB: 6cm * 4cm

With the secondary side the coil is the power source, which delivers an AC signal to the system. For the charging of the ZEBRO an DC signal is necessary. To achieve a DC output an the AC signal has to be rectified. The charger that is connected to the rectifier starts working at a voltage of 6V. The maximum ripple of 0.5V is specified by the BMS team. The charger can malfunction at voltages higher than 32V. In a transformer voltage spikes can cause too high voltages. To protect the charger from breaking down the rectifier output has to limited by an over-voltage protection. There is no need on the secondary side for overcurrent protection because this is done on the primary side. To make sure the secondary side fits inside the ZEBRO the dimensions of the PCB are 6cm*4cm.

2.3. Programme of requirements

This section provides a brief overview of the requirements divided into functional, ecological and system requirements.

A. Functional requirements

(A.1) The system should be able to deliver 100 Watt power to the ZEBRO.

(A.2) The system should have a well-defined interface to the outside world.

(A.3) The system should be expandable for multiple ZEBRO's.

(A.4) The system should charge wireless.

B. Ecological embedding

(B.1) The module should be self-contained.

(B.2) The system may not exceed the limit for human exposure to electromagnetic radiation specified by the ICNIRP. [2].

C. System requirements

(C.1) A damage protection system must be implemented.

(C.2) Measure current and power flow, internal temperature, alignment to station.

(C.3) The system is at the core of the overall system and must be designed with the requirements tabulated in table 2.1.

D. Development of manufacturing methodologies

(D.1) The schematics of the design must be drawn in KICAD or simulated in PSPICE.

(D.2) The final prototypes will be delivered as a PCB design.

(D.3) The design of the system, choice of the components have to be scalable.

E. Business strategies, timespan of the project.

(D.1) The design of the system must be implemented in 5 weeks.

(D.2) The implementation of the whole system must be presented after 11 weeks.

(D.3) A business plan of the whole system has to be presented after 11 weeks.

Overall System	Primary side	Secondary side
General physical dimensions	48 volts input	DC output, max ripple of 0.5V
V_{in} = 48VDC	$I_{p,max} = 2.5A$	PCB dimension (6 cm * 4cm)
V_{out} = 6-32VDC	ZEBRO/FOD detection	Over-voltage protection
$w_0 < 1$ MHz		maximum output voltage of 32V
$P_{max} = 100W$		

Table 2.1: Overview of requirements

3

Theoretical review

3.1. Wireless power transfer types

Wireless power transfer (WPT) is subdivided into radiative (far-field) and non-radiative (near-field). Radiative power transfer is the propagation of EM-waves over long distances. By radiative power transfer the receiver distance r is larger than the transmitted wavelength λ usually where $r > 2\lambda$. Radiative power transfer is subdivided into directive and non-directive. Applications for directive power transmission are for example, a power transmitter (antenna) alongside the road to power electric vehicles. An example of a non directive application is RF harvesting, in which low power devices convert RF waves from the environment into DC. This technique provides a few milliwatts to microwatts [3]. Non radiative power transfer is divided into inductive and capacitive coupling. The capacitive coupling technique is based on creating an electric field between the transmitter and receiver. The space between the transmitter and receiver can be seen as a dielectric, in which the whole system acts as a capacitor. The advantage of capacitive coupling is that it can transfer power through metal. A drawback from capacitive coupling is that the electric field strongly interacts with materials and the human body. Another drawback is that capacative coupling requires a large coupling area. The advantage of inductive coupling is that it has an high efficiency up to 95%. An disadvantage of inductive coupling is that it induces eddy currents though metal. Comparing inductive and capacitive coupling, the latter seems efficient for smaller gap distances of 1 mm [4]. Also capacitive coupling depends on area of the device, which is a design constraint for an optimal power transmission. With all this into consideration, inductive power is the best solution for the WPT for the charging of the ZEBRO.

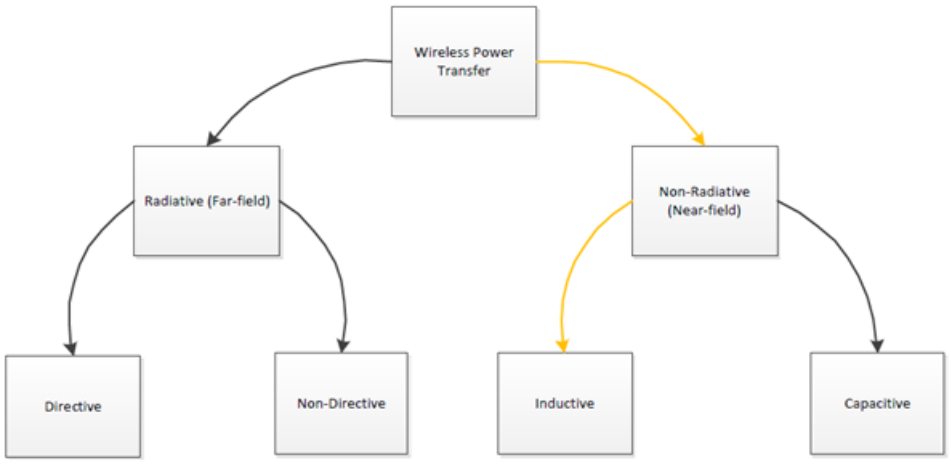

Figure 3.1: Types of wireless power transfer

3.2. Theory

In this section the basic theory [5][6][7][8] of WPT is described. This theory is used to show how to aligned coils affect each other, by the means of mutual inductance. Also the schematic circuit of an inductive power transfer circuit is shown.

The Biot-savart law describes the strength of the magnetic field in a point P, generated by an current. $I\ d\vec{l}$ is a infinite small current carrying segment of a wire, r is the distance from a segment $d\vec{l}$ to the point P and μ_0 is the contsant of magnetic permeability in a vacuum.

$$dB = \frac{\mu_0\ I\ dl\ sin(\theta)}{4\pi\ r^2} \tag{3.1}$$

Consider the two aligned coils from fig. 3.2, whereby only current flows through coil 1. From eq. (3.1) the magnetic flux density B, generated by the current through coil 1 at second coil, is:

$$B = \hat{z}\frac{\mu_0\ I\ N\ a^2}{2\ (a^2 + z^2)^{3/2}} \tag{3.2}$$

$$\Phi_B = \int_s \mathrm{B} \cdot d\mathrm{s} \tag{3.3}$$

where a is the radius of the coil and z is the distance between the two coils, and N is the number of turns the coil has. The generated magnetic field results in an flux Φ_B, eq. (3.3). Faraday's law states that: magnetic flux which changes in time in an closed wire loop will produce an current in the closed loop. The current in the closed loop is produced to create an magnetic field in the opposite direction, to cancel out the change in flux, this is called Lenz's law. The voltage induced by Faraday's law is called the electromotive force (emf). The voltage induced by a closed loop is given by:

$$V_{emf} = -\frac{\partial \Phi_B}{\partial t} = -\frac{\partial}{\partial t}\int_S \mathrm{B} \cdot dS \tag{3.4}$$

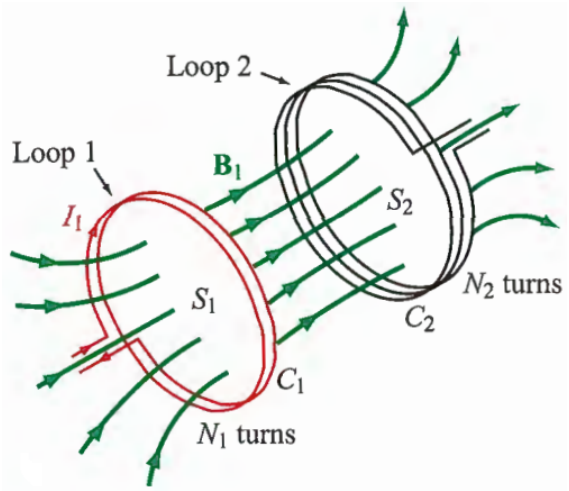

Figure 3.2: Magnetic field lines generated by current I_1 from coil 1 to coil 2 [8]

3.2.1. Self and mutual inductance

The voltage induced by an time-varying current in the same coil is called the self-inductance. The self-inductance is defined as the ratio of magnetic flux to the current flowing to the closed loop:

$$L = \frac{N\ \Phi_B}{I} \tag{3.5}$$

With eq. (3.4) this can be rewritten as:

$$V_1 = L\ \frac{\partial I_1}{\partial t} \tag{3.6}$$

The flux originating from coil 1, Φ_1 has two components: one component Φ_{11} without the interference of an other coil, and second component Φ_{12} that links coil 1 with coil 2 (the magnetic field lines coming out of coil 2 back to coil to coil 1).

$$\Phi_1 = \Phi_{11} + \Phi_{12} \tag{3.7}$$

The induced voltage in the coil 2 is due to the second flux component, Φ_{12}, created by coil 1. Similarly to eq. (3.6) this can be written as:

$$V_2 = M\ \frac{\partial I_1}{\partial t} \tag{3.8}$$

Whereby M is the mutual inductance between the coils described by:

$$M = N_2 \frac{\partial \Phi_{12}}{\partial I_1} \tag{3.9}$$

The mutual inductance of two axially aligned planar coils can be approximated numerically [9][10]. The filament method is used to calculate the mutual inductance. This method first calculates the mutual inductance of two Maxwell loops, which are considered filaments.

$$M = \mu_0 \sqrt{R_1 R_2}\left[(\frac{2}{g}) - g)K - \frac{2}{g}E\right] \tag{3.10}$$

Where K and E are the complete elliptical integrals of the first kind and the second kind to the modulus g, respectively, where

$$g = \sqrt{\frac{4R_1R_2}{(R_1 + R_2)^2 + d^2}} \tag{3.11}$$

Then superposition is used to calculate the mutual inductance of two spiral coils. The current density is assumed to be uniform in every filament. For coils with mulitple windings:

$$M_N = N_1 N_2 M \tag{3.12}$$

The calculation is done in Matlab, the script can be found in the ZEBRO Git.

From the value of the mutual inductance, the grade of coupling between the two coils can be determined. The coupling depends on multiple factors, such as alignment of coils, size and shape the gap between coils. The coupling coeficient k can be calculated with:

$$k = \frac{M}{\sqrt{L_1 L_2}} \tag{3.13}$$

The coupling coefficient defines how much of the total flux is received at the second coil. The coupling coefficient can have an value between 0 and 1, where 0 means no coupling between the coils and a 1 means that all flux generated by the transfer coil is received at the receiver coil. So a higher k means a higher efficiency, another way of describing the efficiency is the quality factor, Q, of a coil. The quality factor depends on the frequency that is applied, a higher frequency results in a higher Q factor. The relation for the Q factor can be written as:

$$Q = \frac{\omega L}{R} \tag{3.14}$$

Where L and R are the inductance value and the resistance of the coil.

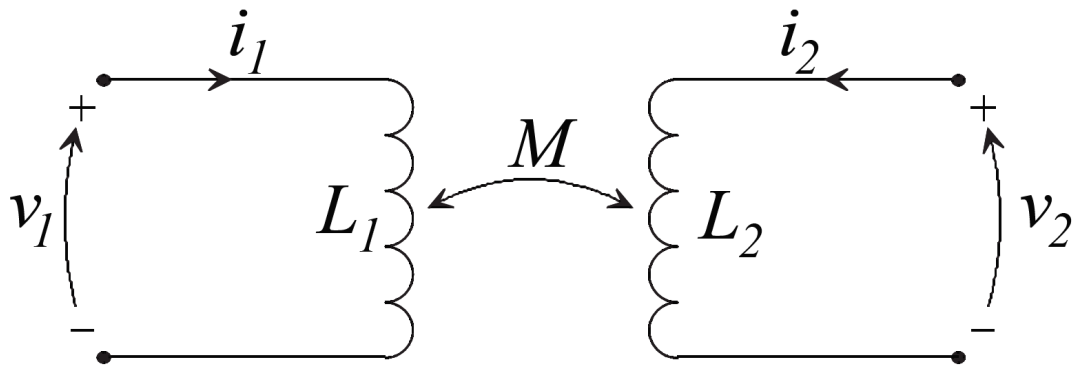

Figure 3.3: schematic circuit of inductive power transfer

In fig. 3.3 a schematic electric network of two mutually coupled coils is shown. With eq. (3.6) and eq. (3.8) the voltage and current characteristics of the two coils can be derived:

$$\begin{bmatrix} V_1 \\ V_2 \end{bmatrix} = \begin{bmatrix} j\omega L_1 & j\omega M \\ j\omega M & j\omega L_2 \end{bmatrix} \begin{bmatrix} I_1 \\ L_2 \end{bmatrix} \tag{3.15}$$

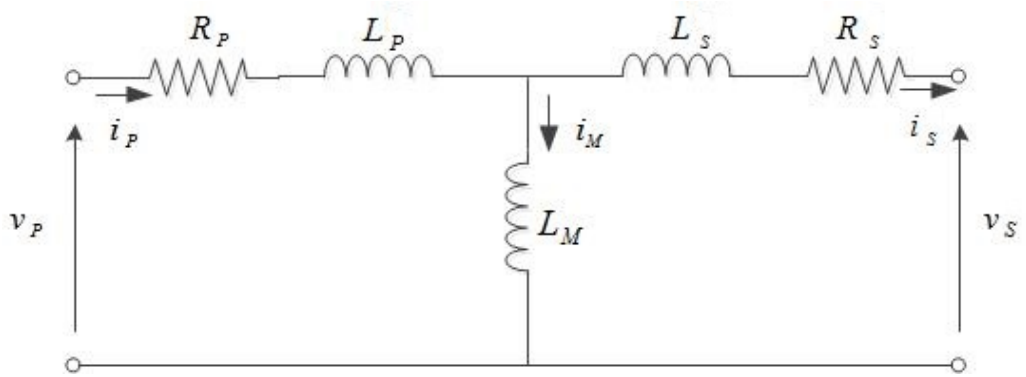

Figure 3.4: Equivalent T circuit of an transformer

The model in fig. 3.3 requires complex calculations regarding the coupling factor. It is therefore more convenient to replace the magnetically coupled circuit with an equivalent T model transformer without magnetically coupling. The equivalent T circuit is depicted in fig. 3.5. Whereby R_P and R_S are the parasitic resistances of the primary and secondary coil. L_P and L_S are the non-coupled leakage inductance's $L_1 - M$ and $L_2 - M$.

3.2.2. Compensation capacitors

There are two types of inductive power transfer: closely coupled systems and loosely coupled systems [11]. An example of the closely coupled system is a transformer with a solid core. The efficiency improves with a shared core between the coils, but the downside of this is that the coils can not be seperated easily. A loosely coupled system provides a gap between the coils, which makes it practical for movable coils. Because of the gap between the primary side and the secondary side the mutual inductance will be smaller. A smaller mutual inductance leads to higher leakage inductance. The leakage inductance affects the efficiency of the power transfer. To compensate for the leakage inductance, compensation capacitors are needed such that the impedance at the secondary side will be purely resistive [12][13]. For a LC-tank the impedance seen from the source can be expressed as follows.

$$Z = \frac{1}{j\omega C} + j\omega L \tag{3.16}$$

From the previous statement, the following relation holds: $Z_{imaginary} = 0$. From this, the capacitance at the secondary side can be derived.

$$C_2 = \frac{1}{\omega_0^2 L} \tag{3.17}$$

Where ω_0 is the operational resonant frequency. The primary capacitance is dependent on the topology used. The four compensation topologies that are the most used are: series-series (SS), series-parallel (SP), parallel-series (PS) and parallel-parallel (PP). The topologies differ in the series (S) or parallel (P) placement of the capacitors. The primary compensation is independent of the load if the primary compensation is series compensated [14] A general conclusion can be made that the SS-topology has the

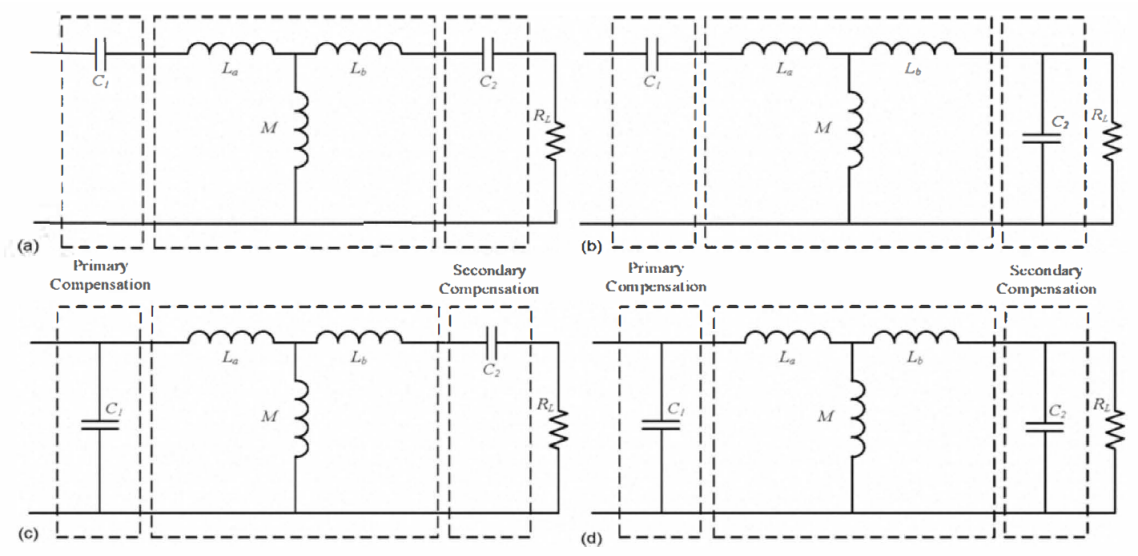

Figure 3.5: The four compensation topologies,(a) SS, (b)SP,(c)PS,(d) PP [15]

advantage that the primary capacitor value is independent of the mutual inductance and the load [15]. However, some studies argue that the SP topology is best suited for the battery charging application. In [16][12] it is discussed that the SP compensation acts as a constant current source, whilst the SS variant acts as a constant voltage source. In fig. A.1 the value for the primary capacitor is specified per topology.

3.2.3. Power inverter topology

The conversion from DC to AC can be done with an H-bridge. H-bridges can be implemented as a full or half bridge, the full bridge consists of four switches. For the half bridge, switching the upper and lower transistor on and off the current changes direction through the load. For the full bridge switching on a diagonal pair of switches also changes the direction of the current through the load. In fig. 3.6 an implementation of the full and half bridge is shown.

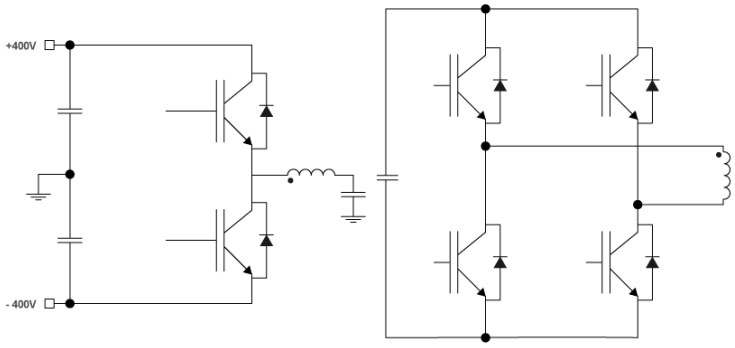

Figure 3.6: H-bridge topologies (Infineon)

It is to be concluded that the half bridge requires a negative and positive input voltage with respect to the output neutral. In some applications this is not an issue. Design restrictions could imply less use of transistors which would favor the implementation of a half bridge. The full bridge does not need a positive and negative input voltage. The full bridge consists of two half bridges which increases the amount of transistors. A design trade-off has to be made for choosing the implementation of the inverter, this will be done in section 4.2.1.

3.2.4. Primary side control

When the system is operating at a fixed frequency, changes in the load seen from the source will have an effect on the power transfer [17]. Also a fixed frequency system would not always operate at zero phase angle of the power supply, the phase difference between the power supply voltage and current will not be zero. This decreases the efficiency of the power transfer. Variable frequency control minimizes the required VA rating of the power supply. This can be accomplished by controlling the frequency such that the phase difference between the power supply voltage and current is always zero.

Phase detection

The first step in controlling the frequency of the system is to measure the phase difference between the voltage across the coil and the current through the coil. Current measurement is done by a shunt resistor. Using an ADC can complicate the design process of measuring and controlling the system. The high frequency AC signal would need a high sampling rate. Therefore, hardware can be used to detect the phase difference between the voltage and current waveforms. The current is measured using a shunt resistor. Shunt resistors are low resistance devices used for current sensing. Voltage sensing is done by using a voltage divider circuit. A comparator compares the input signal with a specified threshold. When the input signal is above the threshold the comparator outputs a high signal and when the input signal is below the threshold the comparator will output a low signal. When both the voltage and current measurements, are linked to a comparator the phase difference can be found when both outputs of the comparators are linked to a exclusive-OR.

When the voltage and current waveforms are measured a controller has to be implemented for varying the frequency. Several control methods are available for variable frequency control [18]. However, to keep the implementation relatively simple a similar method described in [19] can be used for finding the optimal frequency.

3.3. Safety

As stated in requirement B.2 the WPT system has to meet the safety standards as defined by the International Commission on Non-Ionizing Radiation Protection (ICNIRP). High frequency (HF) is defined as the part of electromagnetic spectrum between 100kHz and 300GHz. The relevant safety effect from HF fields to the human body is the heating of exposed tissue. When HF fields penetrate the human body, vibrations of charged molecules causes friction and thereby creates heat. The human body can handle a small increase of heat, but above a certain threshold the temperature rise can have serious safety effects like a heatstroke or tissue damage. Nonetheless, when the guidelines for safety according to the ICNIRP are followed the mentioned affects should not happen. In fig. 3.7 a graph of the safety standard for the magnetic field is depicted. It is clear from this graph that the maximum acceptable flux density decreases as the frequency increases. From the graph a good estimate is that the frequency should be $100kHz$, the maximum acceptable flux density will be $6.25\ \mu$B. To test if the wireless charging pad satisfies the safety conditions, a EMC−scan should be made.

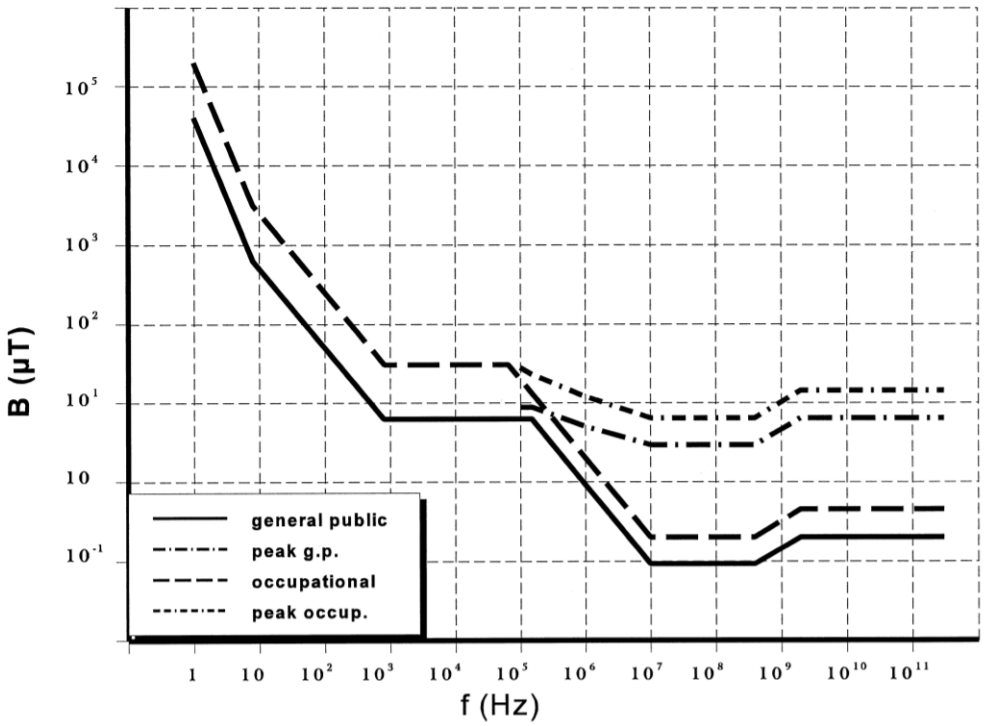

Figure 3.7: Safety standard for the magnetic field by the ICNIRP [2]

3.4. State of the art

Wireless power chargers are already used for a while in consumer goods. Probably one of the most well know examples is the electronic toothbrush, the wireless charging advantage is that the system can be waterproof. Lately, the market of wireless charging devices is growing rapidly, mainly because of the integration of the technology in smartphones. A wireless power charging standard will help the technology to be faster adapted. This is because it is easier for companies to integrate it in their product. Standards are used in technology to ensure the safety and reliability of a product. Also, standards are used to make sure products are compatible with other products from the same standard. In the current market of wireless charging there are different wireless power transfer standards. The two main alliances are: Wireless Power Consortium (WPC) with 'Qi'[20] and the Airfuel Alliance [21] with 'Airfuel'. Those standards are not compatible with each other, but some devices support multiple standards.

Qi

The WPC, which developed 'Qi', was established in 2008. It is the largest alliance with 214 companies supporting the qi standard. the Qi standard has open specifications for their newest low power applications, which support 5-15 Watt of power transfer. For communication between the charging pad and receiver inbound communication is used, via Amplitude Shift keying.

Airfuel

Airfuel Alliance is created by the merger of the Alliance for Wireless Power (WP) and the Power Matters Alliance. Airfuel is mainly based on the rezence standard from A4WP. The Rezence standard [22] supports a power transfer of 50 watts and can charge multiple devices at once. To make the charging pad communicate to the receiver, outbound communication is provided via an Bluetooth module.

4

Design

In this chapter the design of the system is discussed. In the first section an overview is given of the total design, where the system is divided into subsystems. In the next section these subsystems will be discussed in detail. In the last section the use of the subsystems are discussed.

4.1. Overview

The input of the WPT is a DC voltage. This has to be converted into AC to induce a voltage in the secondary coil. The induced voltage has to be rectified at the secondary side to provide a DC voltage to the battery. The coils, the inverter and rectifier are the essential parts of the WPT system. The effiency is improved by implementing a compensation network. The compensation network improves the efficiency by decreasing the reactance due to the inductance of the coil. The V/I-sense will measure the current and voltage through and across the coil. This provides a framework for further improvement of the design. In fig. 4.1 an overview is given of the subsystems.

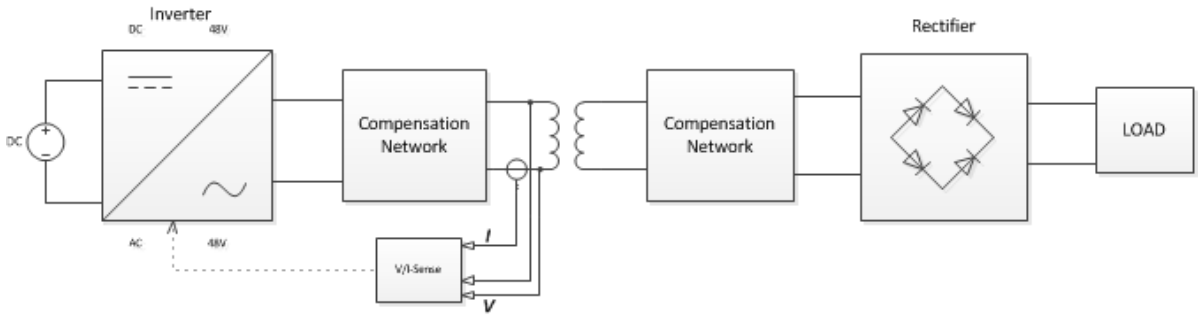

Figure 4.1: Overview of the WPT subsystems

4.2. Detailed design

In this section the design choices of the subsystems are explained. As explained above, the system consists of four main parts. The inverter, coils and compensation, rectifier and voltage and current sensing.

4.2.1. Inverter

The inverter is the first part of the system. The input is 48 volts DC and the output of the inverter has to be high frequency 48 volts AC. The frequency of the inverter is chosen to be 100kHz. The following section explains this design choice, since the resonant frequency is dependent on the coil and compensation network. Other methods [10] exist to provide an AC signal to the transmitter coil. The full H-bridge is chosen because it is often used and the amount or physical size of transistors is not limited in the design.

The MOSFETs need to switch at a certain frequency. This is done by a Pulse Width Modulator (PWM) which generates a signal at the desired frequency and a duty cycle. The MOSFETs will not switch with a small gain current. Therefore, gate drivers are needed to switch the MOSFETs. Also, components such as MOSFETs and resistors are chosen such that the currents and voltages do not damage the components.

LM5054

The LM5045 [23] is used as gate driver and frequency generator. The chip contains a PWM generator and gate drivers. Also, dedicated pins are able to detect under and over-voltage at the input of the inverter. The LM5054 uses pin 1 and 2 to detect if the input voltage exceeds or is under a certain threshold value. The threshold is fixed by dividing the voltage over the pins. When pin 1 (UVLO) exceeds 1.25 volts the devices is turned on. When pin 2 (OVP) exceeds 1.25 volts the device is turned off. The under-voltage limit is chosen to be 16 volts, the over-voltage limit 52 volts. The Current Sense (CS) pin terminates the PWM cycle when the voltage across the pin exceeds 750 millivolts. A shunt resistor is connected at the low side of the H-bridge. When the voltage across the resistor exceeds 750 millivolts the device is shutdown. For filtering out unwanted frequencies a RC-filter is used between the CS pin and the resistor. The cut-off frequency of the RC filter is chosen to be $f = 10kHz$. This is the maximum cut-off frequency since the first order filter has a -20dB/decade slope. For the PCB design, the filter components should be located close to the chip since radiated noise could affect the measured current. Another feature of the LM5045 is the possibility to vary the frequency and the duty cycle of the PWM signal. This is done through an external clock source into the RT pin or by varying the current into COMP pin, respectively. These pins will be available on the PCB for further improvement of control on the primary side of the system.

The under and over voltage protection, voltage dividers for the chip are R_1, R_{UVLO} and R_{OVP}. Values for these resistors are determined by the following equations:

$$R_1 = \frac{V_{hys}}{20\mu A} \tag{4.1}$$

$$R_{UVLO} = \frac{1.25 \cdot R_1}{V_{PWR} - 1.25 + (20\mu A \cdot R_1)} \tag{4.2}$$

$$R_{OVP} = \frac{1.25 \cdot R_1}{V_{PWR_{OFF}} - 1.25 - (20\mu A \cdot R_1)} \tag{4.3}$$

Where V_{hys} is chosen to be 2 volts to prevent the device switching on and off at the threshold voltage.

A 100 kΩ resistor is connected to the RT pin to produce a frequency of 100 kHz. For the gate drivers, bootstrap capacitors and diodes are connected to pins BST and HS1 and HS2. The bootstrap configuration ensures a correct gate-source voltage across the MOSFETs [24]. The HS pins are connected between the high and low side of the H-bridge. When the HS pin is pulled to ground, the bootstrap capacitor is charged from the VCC supply. The BST pin will thus be supplied. When the HS pin is pulled up to a higher voltage, the diode is in reverse bias and the BST pin will float, thus blocking the rail voltage from the supply. For the MOSFETs the 530N15N NMOS transistors are used. Which are capable of a drain-source voltage of 150 volts and allow a 21 A drain current. For over-current

protection, a shunt resistor is used to measure the current through the low side of the H-bridge. In appendix B.1 an overview is presented of the used components for the inverter. Also in appendix B.2 the schematic is to be found of the topology of the inverter.

Current and Voltage Sensing

Current sensing allows the possibility of load detection. The current through the primary coil changes when an inductive load is present near the primary coil. For control applications at the primary side, current and voltage sensing is implemented. The basic idea is that the current through and the voltage across the coil will be measured. This is done by a shunt resistor in series with the load for measuring the current. A shunt resistor is of low resistance and minimizes the influence it has on the load. The signal has to be amplified, a choice has to be made whether the current sensing will be done inline or at the high or low side [25]. For the over current protection, the low side of the H-bridge is measured, because of simplicity the sensing method. For the control application, inline current sensing will be used. The voltage measurement is done by voltage dividing the voltage across the coil. The signal has to be amplified before it is processed. It is important to note that inline current sensing requires an amplifier with a wide common mode voltage range. This is because of the over and undershoot of the PWM. For the design of the PCB, the pins are made available to measure the current and voltage and alter the frequency and duty cycle of the PWM. This makes it possible to improve the efficiency of the system and detecting the presence of a Zebro.

4.2.2. Coils and compensation network

The design of the coils can be optimized with help of simulation software. The process of designing optimal coils for the given application is an iterative process and requires an extensive study in itself. Design guidelines for coils exist that optimizes the power transfer [26]. The outer shape of the coil, the diameter of the wire, the separation of the windings and the number of turns do not have a significant influence on the coupling factor k. However, other parameters do have a significant influence on the coupling factor which are listed below.

- The outer shape of the receiver coil should be maximized to the receiver's area.
- The inner radius of the transmitter coil should be minimized.
- The transmitter coil radius should be greater than the receiver coil radius.
- Minimizing the diameter of the wire decreases the quality factor of the coil.

These design rules helps for optimizing the coupling factor k between the two coils. The quality factor Q can be optimized by varying the diameter of the wire, the spacing between the turns can affect the operating frequency of the system. Litz wire is used to minimize the effect of the high frequency AC through the coil. The phenomena 'skin effect' causes an increase in resistance of the wire at higher frequencies. Optimizing the design of the coil, also affects the design of the whole system. For the scope of this project, the design of the coils is kept to a minimum.

Coil design

For the sake of simplicity the coil is chosen with respect to the form factor and the availability. The winding ratio of the coils is 3:1 to guarantee that the 48V at the primary side is 16V at the secondary side. The mutual inductance of the coil can be calculated via numerical methods. In the Zebro GIT a Matlab script can be found that numerically calculates the mutual inductance, knowing the inner and outer radius of the spiral coils. The charging pad and the ZEBRO limit the area the coils can cover. Therefore, the following dimensions are chosen with respect to the inner and outer radius of the coils.

Table 4.1: Coil dimensions

	Primary coil	Secondary coil
Inner radius (mm)	250	500
Outer radius (mm)	750	650

The inductances of the coils depend on the geometry and the physical parameters of the coil. The coil is wound with Litz wire with a diameter of 1.8mm. These values result in an inductance of $L_1 = 97\mu H$

and $L_2 = 20\mu H$ and a mutual inductance of $M = 30\mu H$ For an optimal design of the coils, the design guidelines in the previous section and the method in this section should be used to obtain the mutual inductance of the coils.

Compensation topology

Compensation is needed such that the reactive power consumed by the circuit will decrease. This is done by adding capacitors at primary and secondary side of the coils. Different topologies are possible. For the application to charge a battery, the SS-topology is chosen. The SS-topology is optimal for battery charging applications where misalignment is an issue[15]. The WPT acts as a constant voltage or constant current source which is preferred when charging a battery. Also, the compensation capacitors will be independent of the mutual inductance and the load. For this topology, the capacitor values only rely on the self-inductances of the primary and secondary coils. This is desirable when misalignment is an issue, in which the mutual inductance varies with respect to the position of the coils.

For the SS topology the power delivered and the efficiency of power transmission to the load can be defined as [27]:

$$P_{out} = \frac{V_{in}^2 \omega^2 M^2 R_L}{(R_1(R_2 + R_L) + \omega^2 M^2)^2} \tag{4.4}$$

$$\eta = \frac{\omega^2 M^2 R_L}{R_1(R_2 + R_L)^2 + \omega^2 M^2 (R_2 + R_L)} \tag{4.5}$$

Where R_1 and R_2 are the resistances of the coils. These AC resistances can be calculated [28] or measured. The compensation capacitor at the secondary side can be calculated with the following equation:

$$C_{secondary} = \frac{1}{\omega_0^2 L_s} \tag{4.6}$$

Where ω_0 is the operational frequency that will be determined in the next section. The primary capacitor can be calculated with the following equation:

$$C_{primary} = \frac{1}{\omega_0^2 L_p} \tag{4.7}$$

Operational frequency and capacitor values

The compensation network determines the self-resonant frequencies of the primary and secondary side. The circuits can be analyzed as LC-tanks. The system has to switch at the self-resonant frequency of the secondary side. This is to reduce the reactive power seen from the source. For design purposes, first an operational frequency is chosen. Based on this choice, the components are chosen to fit the operational frequency.

The operational frequency is chosen, by considering the efficiency of the system. In the previous section the efficiency is mathematically derived. For the design process, a mutual inductance of $M = 30\mu H$ is used. A logarithmic graph is plotted with varying values of R_{load} in ohms.

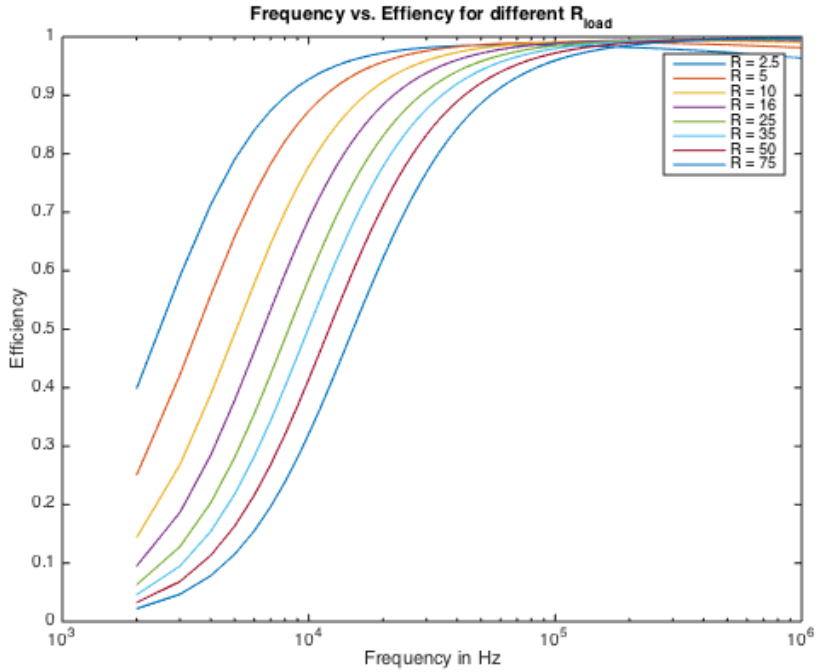

Figure 4.2: Efficiency as a function of the frequency. R_{load} is displayed in ohms.

The figure shows that an optimal frequency for a varying load between 2.5Ω and 75 Ω is 180 kHz. For safety reasons specified in the requirements (B.2) and discussion in section 3.3 the system should not exceed a frequency of 150 kHz. Also, according to the BMS requirement (C.3) the operating frequency should be $<$ 1 MHz. Therefore, the operating frequency is chosen to be 100 kHz. Further analysis is done in appendix D, where the coupling factor of the coils is compared with respect to the frequency.

4.2.3. Rectifier

A full bridge diode rectifier is used to rectify the sinusoidal signal induced by the secondary coil. The diode bridge is a form of passive rectification. The alternative was active rectification, with a synchronized rectifier which has a higher efficiency. In the synchronized rectifier the diodes from the passive rectification are changed with active controlled switches. The diode bridge has a lower efficiency, because of the voltage drop over the diodes. The advantage of the diode bridge is that it does not need a controller to control switches as in an active rectifier, which also saves space. From the requirements the output voltage should not be able to go above 32 volts, to achieve this, over voltage protection limits the output of the rectifier.

Diode Bridge and smoothing capacitor

A diode is a component that lets current only flow in one direction. In the H-bridge configuration the diodes flip the negative side of the sinusoidal signal to the positive side, creating a full ripple DC signal. For the rectifier to be efficient it is important that the diodes have a low voltage drop and a low internal resistance. Schottky diodes are a type of diode that have a low voltage drop and have a high switching speed in comparison to pnjunction diode. The disadvantage of a Schottky diode is that the breakdown voltage is limited [29], to overcome this issue Silicon Carbide Schottky diodes can be used[30].

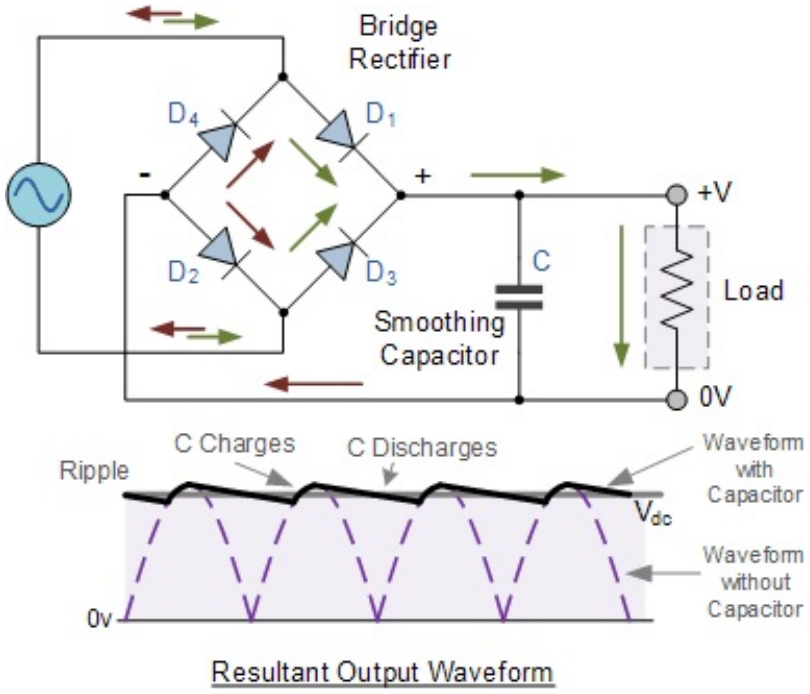

Figure 4.3: Full bridge rectifier with smoothing capacitor [31]

$$I_c = C\frac{dV}{dt} \Rightarrow C = \frac{\int I_c dt}{V} \tag{4.8}$$

$$C = \frac{I_{load}}{f * V_{pp\ ripple}} \tag{4.9}$$

To keep the output voltage as constant as possible, a capacitor can be used. From the requirements in section 2.2.2 is determined that the ripple should not be more than 0.5V. The capacitor smooths the full ripple signal to a steady DC signal by discharging the capacitor when the rectified waveform goes down. The ripple caused by the discharging of the capacitor is given in eq. (4.8)[31]. I_c is the capacitor current, C is the output capacitance of the capacitor, $\frac{dV}{dt}$ is the change in voltage over the time the capacitor discharges. eq. (4.8) can be written as eq. (4.9), from this can be seen that the ripple not only depends on the capacitor but also on the frequency.

When designing the capacitor compensation eq. (4.4) is used to check if the output power is the same as the required 100W, which is the case. The simplified model used for the power output calculation is too basic too say something about the actual power transfer circuit with rectifier. In the simplified model the load of 16Ω specified by the battery management system team looked good to achieve the power transfer of 100W. But, when the input of the rectifier is seen as a sinusoidal 16V 100kHz source, the output voltage is a steady 16V when the losses of the of the diodes are neglected. With a 16V output and a desired output power of 100W the output impedance should be rated at 2.56Ω, instead of 16Ω, the current is then 6.25 Amps. Impedance matching can be performed to reach a higher power transfer. For the design of the capacitor I_load = 6.25A is used, because this will result in an 100W output power at 16V. If the current is lower, but the capacitor is still designed for 6.25 Amps the ripple will always reach the requirement of a ripple of 0.5V.

$$C = \frac{6.25}{10^5 * 0.5} = 125\mu F \tag{4.10}$$

To decrease the equivalent series resistance (ESR) of the capacitors multiple capacitors should be placed in parallel.

Over voltage-protection

According to the requirements in section 2.2.2 the output of the WPT system has to limited to 32 volts. To achieve this the circuit has to automatically switch off the supply to the load when the limit is reached. The transistor is an electrical component which can be used as electrical switch. The on/off state of a transistor is determined by the gate voltage. To control the gate voltage another transistor is used. This second transistor only conducts when there is a voltage difference over resistor R1, shown in fig. 4.4. There will only be a voltage difference over the resistor when the input voltage of the over-voltage protection is higher than the break down voltage of the Zener diode. The Zener diode is a diode that operates like a normal diode until a specified voltage is reached, the breakdown voltage, then the Zener diode also works in the reverse direction.

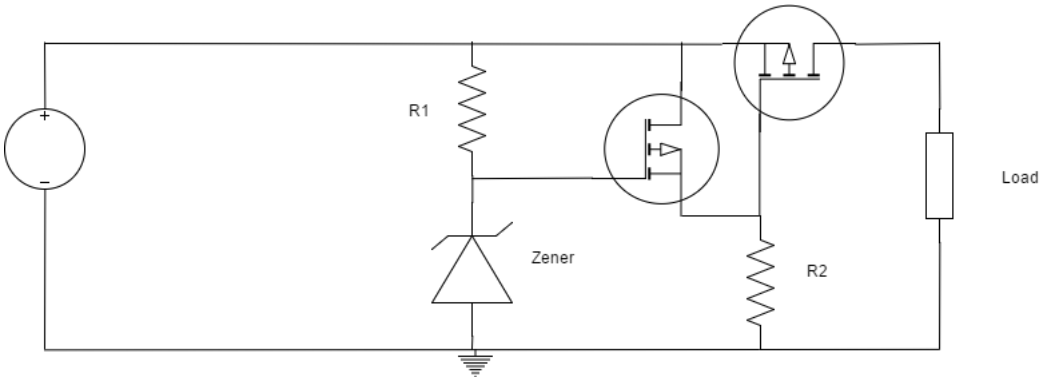

Figure 4.4: Circuit design of Over-voltage circuit

Simulation

All the images of the models and simulation are in appendix C. To assess whether the selected design would work as expected, models were made of the circuits of the rectifier and overvoltage protection in LTspice XVII, as seen in fig. C.1 and fig. C.2. After both parts worked as expected an model was made of the rectifier with overvoltage protection, shown in fig. C.3.

To test the model of the overvoltage protection, an impulse signal is given as input. The input signal starts at 25V and after 5ms the input signal rises to 35V. From the output signal, shown in fig. C.4, it is clearly seen that as the voltage after 5ms at the input goes up, the output voltage drops down to 0V. This illustrates that the overvoltage protection works.

The diode bridge rectifier is simulated by providing a sinusoidal voltage source of 16V at the input, in fig. C.5 the simulated output is shown. The load resistance is 16Ω, and the ripple is 0.5V. According to the calculated smoothing capacitor the ripple should be lower than 0.5V, because the current is approximately 1A. With this knowledge, that the ripple is not as expected by the calculation in eq. (4.10), more value must be attached to simulations than to the calculation.

In the simulation of the whole rectifier, the diode bridge and overvoltage protection, the capacitor value is higher than calculated which results in an ripple of 0.4V. In fig. C.7 input and output signals of the whole system are shown, when a 16V 100kHz signal is delivered at the input. To test the over-voltage protection of the rectifier a 35V 100kHz signal is delivered at the input. In fig. C.8 it is seen that the overvoltage protection starts working as expected at an output voltage of approximated 32V. To also test if the overvoltage protection protects the system of voltage spikes, a DC input signal with an impulse is simulated for the whole rectifier. The input signal is changed from an steady 16V input to an steady 35V input. As seen in fig. C.9 voltage spikes will not go above 32V. When the voltage increases to larger values than 35V the peak of the voltage spike will not go above the 32V, the only thing that happens is that the spike becomes narrower.

5

Prototype implementation

In this chapter the design is implemented into hardware. In the following sections the prototypes are discussed, the test plan is executed and results are discussed. Further on, conclusions are drawn on the entire project and possible future work is treated.

For testing purposes, the system is again divided into three parts. Each subsystem is tested with the proper inputs and measured at the output. The inverter has to be tested to verify if the requirements are met, such as the DC to AC inversion, the overcurrent protection, the shutdown and turn on voltage levels. The coil design is verified by measuring the inductances of the wounded coils and by measuring the mutual inductance of the coils. The verification will be done by comparing the measured values with the calculated values. The rectifier is tested for the requirements set in the previous chapter. These include rectifying the signal, over-voltage protection and the percentage of ripple in the rectified signal. The prototypes are built to verify the functionality of the designs, a further design iteration is needed to get production-ready hardware. Form factors of the prototypes are not suitable for implementing in the rest of the system.

5.1. Prototype

5.1.1. Inverter

The prototype is built on an experiment board with through hole connections with relatively small diameter wires. This prototype would not be optimal for the required power transfer. However, the prototype is built to test the behaviour of the IC. The LM5054 is bought in a 28TSSOP package since this was readily available. An adapter is used for the 28TSSOP package. The prototype board is depicted in fig. 5.1.

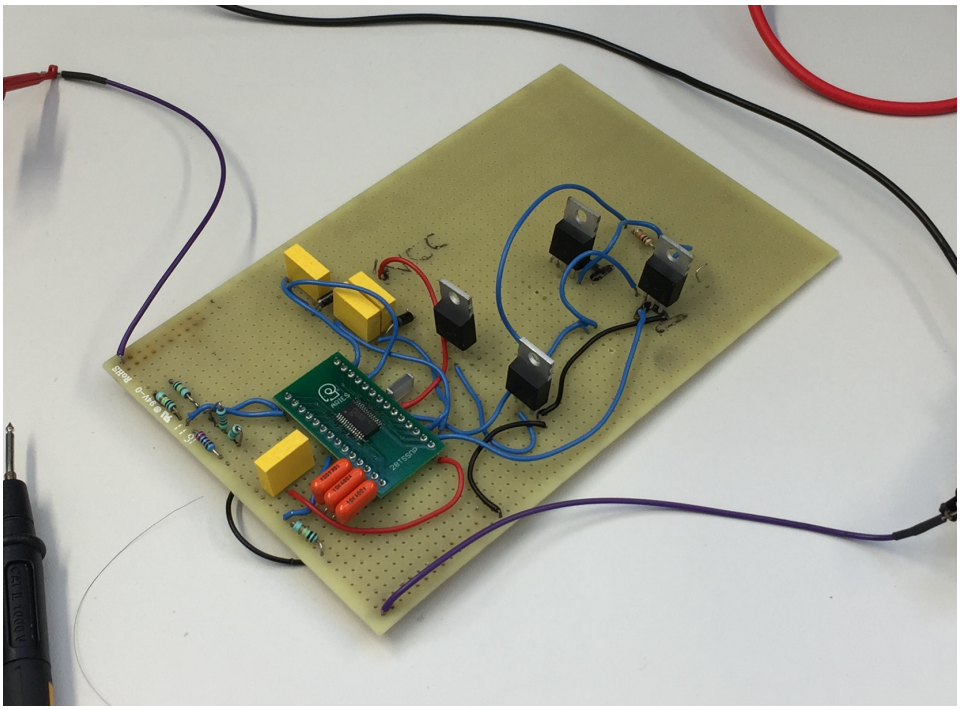

Figure 5.1: Inverter prototype

5.1.2. Coils and compensation

The coil dimensions specified in the design are wound and the inductances are measured with an LCR-meter. The measured inductances, mutual inductance of the coils are to be found in table table 5.1. The mutual inductance is measured with the coils axially aligned and with a vertical distance of 5 mm. The capacitor values are dependent on the availability of the components. Therefore the following values are chosen. The calculated mutual inductance $M_{calc} = 26\mu F$ corresponds with the measured mutual inductance with an error of 13.3 percent.

Component	value
L_p	97 μH
L_s	20 μH
C_p	12.7 μF
C_s	270 μF
M	30 μH

Table 5.1: Values coils and compensation capacitors

5.1.3. Rectifier

After the simulations verified the designed circuit, a prototype was implemented on an experiment board, fig. 5.2. For the prototype of the experiment board, off the shelf components were used that were available at the lab. One main difference of the simulated model and the one on the experiment

board is that the Zener diode on the experiment board is 5.6V instead of 30V, when the input signal is above the $5.6V+$the $V_{threshold}$ of the PMOS transistor the overvoltage protection will start working. The PMOS that is used on the board is a IRF9530 Power MOSFET [32]. The threshold of the IRF9530 is between the 2V and 4V. It was possible to get the Zener voltage to 30V by putting them in series, but the used function generator can only deliver small power signals so there was only one Zener used. Also because the function generator can only output small power AC signals the ripple is not tested with this prototype.

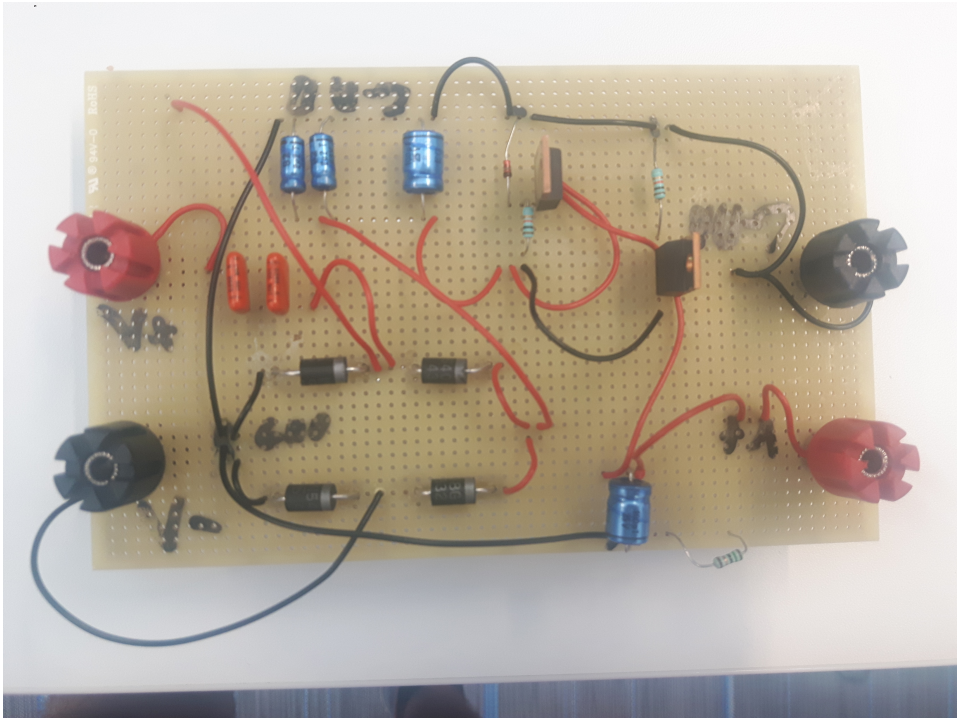

Figure 5.2: Rectifier prototype

5.2. Testing and results

This section presents the testing of the prototypes and results obtained by measuring the output of the prototypes. Also, test setups are presented and discussed.

5.2.1. Inverter

For testing purposes the inverter is connected to the Agilent E3611A DC Power Supply with a limited output voltage of 35 volts. A resistor is connected at the output of the inverter to measure the output characteristics of the inverter. The resistor chosen for this test is 250 Ω. The over voltage and under voltage lockout is tested by changing the input voltage of the power supply. The signal at the load is measured with a Tektronix TDS 2022C digital oscilloscope.

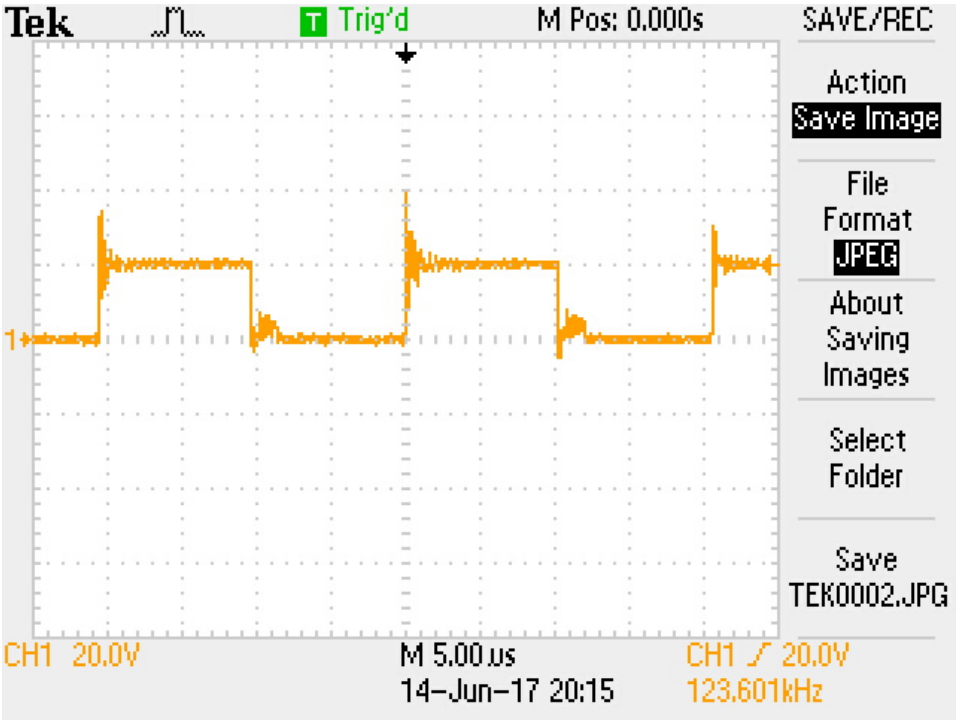

Figure 5.3: Oscilloscope output of the inverter

The figure shows an output waveform of 20V when the input voltage was set to 20V. The expected frequency with the R_t resistor was 100 kHz. The scope measures a frequency of 123 kHz. This could be due to the resistance or to the build of the prototype. The problem persisted when changing resistors. A solution to this problem could be a robust PCB design or connecting an oscillator to the RT pin. The output waveform shows noteworthy unstable switching. The overshoot is about 60 percent of the amplitude of the signal. This could be due to the load which is purely resistive or because of the hard switching of the chip. Soft switching is not enabled in the chip and could be used as an improvement. Also, the start up of the inverter is not as expected. A solution to this problem would be a pi filter, which is also recommended in the data sheet.

5.2.2. Rectifier

After the rectifier was soldered onto the experiment board it could be tested on its functionality. To supply an AC signal of 100 kHz to the prototype an AFG3021C function generator was connected to the input. The output was measured via a Tektronix TDS 2022C digital oscilloscope. At fig. 5.4 the test setup is shown. The output voltage of the function generator was also measured on the oscilloscope to make sure that the expected output came from the function generator. In fig. 5.5 is seen that when an input voltage of 7.5V is applied to the circuit that a steady output is generated that is around the 6.5V. The next figure, fig. 5.6 shows that the output voltage reaches an estimated value of 8V. This is still reasonable because the maximum threshold voltage of the PMOS is 4V and the breakdown voltage of the Zener is 5.6V, which results in a maximum allowable voltage of 9.6V. In fig. 5.7 it is seen that when the input voltage exceeds 10V the output goes down, because the overvoltage protection is activated. The test results show that the overvoltage protection works as expected and the output gets rectified.

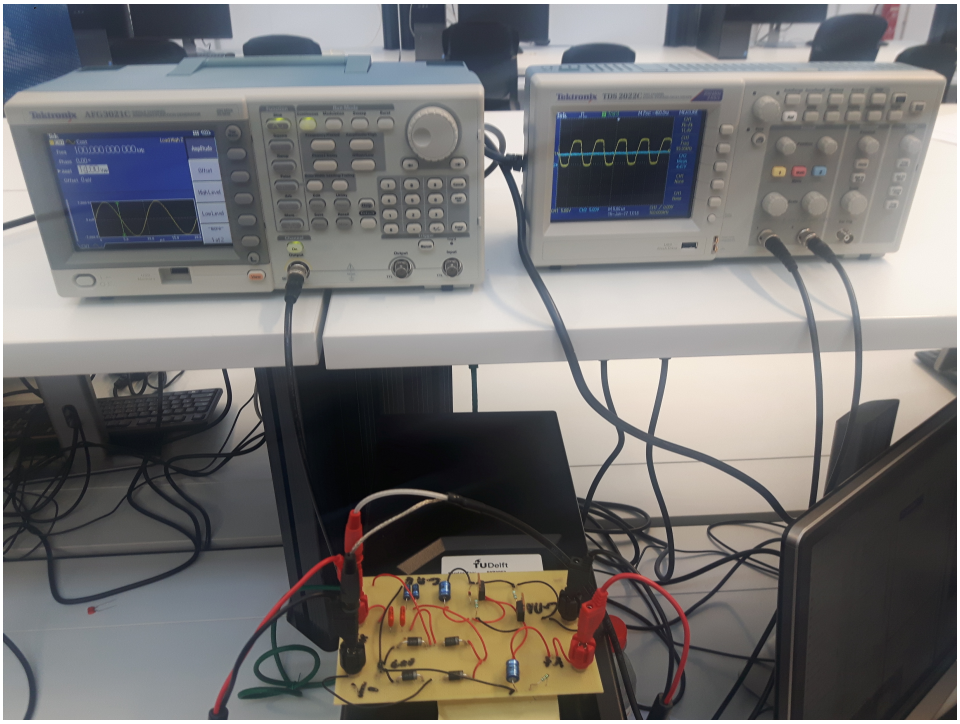

Figure 5.4: Test setup for the Rectifier

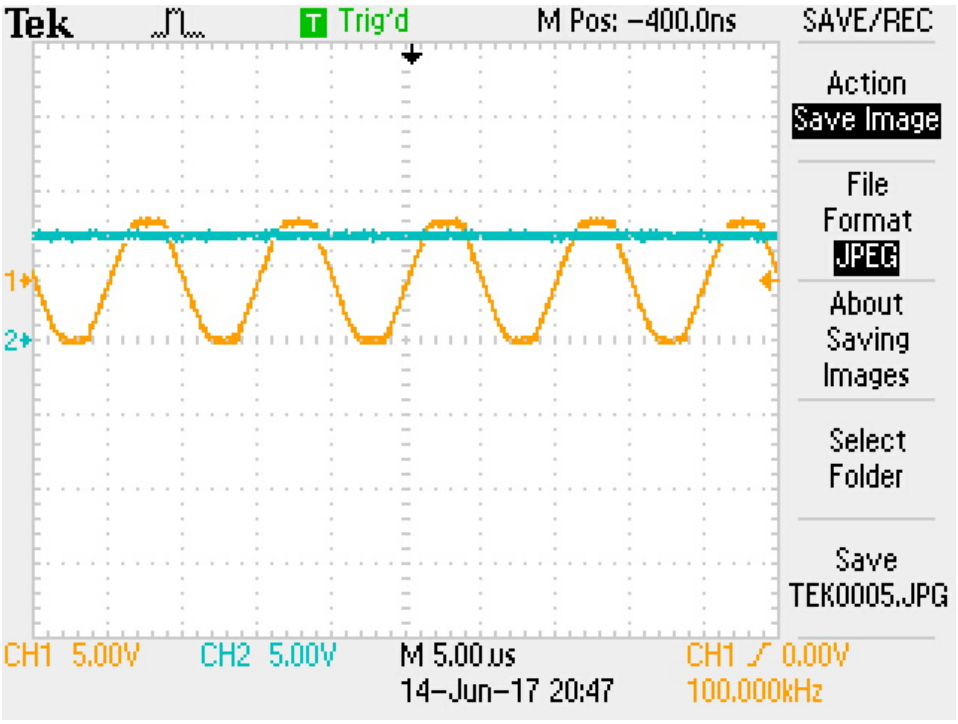

Figure 5.5: Rectifier prototype test, CH1:input, CH2:output, the overvoltage protection is not active

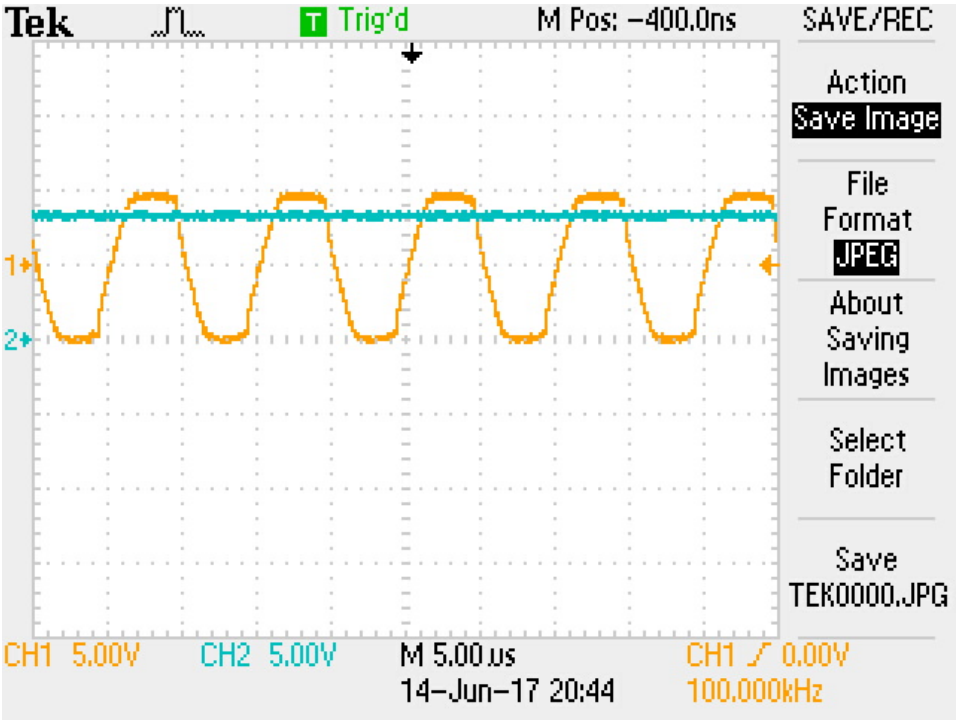

Figure 5.6: Rectifier prototype test, CH1:input, CH2:output, the overvoltage protection is not active

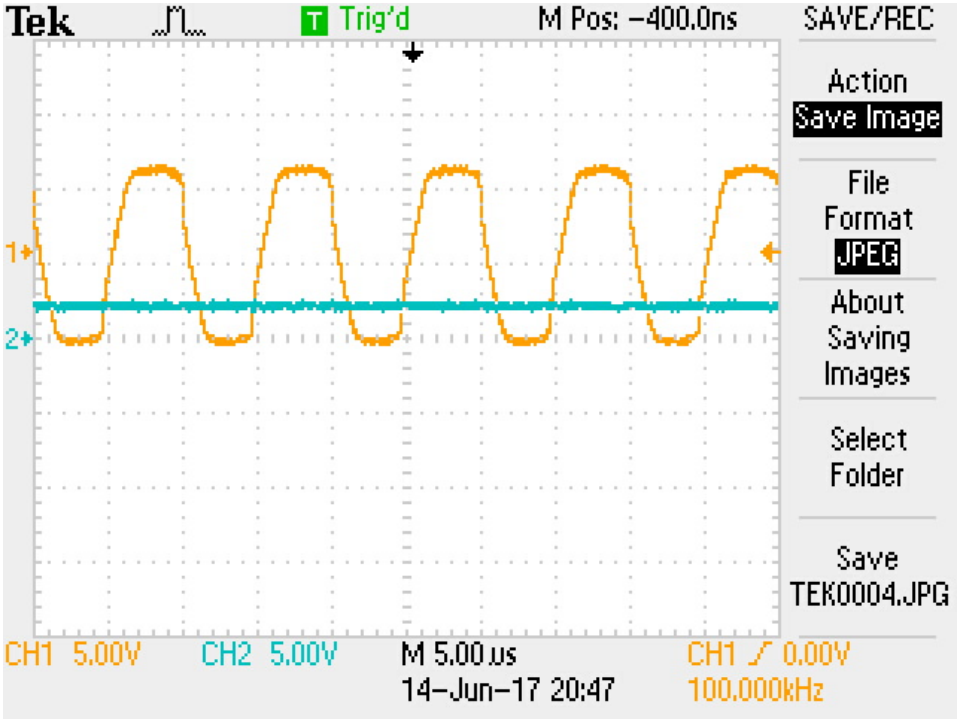

Figure 5.7: Rectifier prototype test, CH1:input, CH2:output, the overvoltage protection is active

6

Conclusion and Recommendations

The design process and the evaluation of the prototypes will be discussed in this section. Further on, recommendations and future work will be treated for improvement of the system.

Design Process

The WPT system design is an iterative design process, since all the subsystems influence the parameters of the other. Therefore, a lot of time was spent searching for an optimal design method for the given application. Several articles exists that provide a guideline for designing a WPT system, which are included in writing this thesis. The focus of the thesis was set on improving the primary and secondary side of the system to meet the requirements. The result of the design process is a functioning inverter, topology of compensation and a rectifier that meets the system requirements. Implementation of the basic design needed a lot of debugging. Improvement of the basic system is not implemented. Therefore, the design proposed in the thesis is to be used as framework for improvement of the WPT system. Improvement is done by the theory provided in the thesis and the expandable design of the PCB.

Evaluation of the prototypes

The prototypes presented in the thesis are tested on the functionality of the designs. These functionalities are validated and will be built upon. The actual PCB designs will have to consider the area of the traces to allow the required power transfer. Also, placement of the components and heat sinks for transistors have to be taken into account for designing the circuit. The prototypes need an iterative design process to be production-ready for the overall system. The overall system will be tested when the PCB designs are implemented.

Future Work

The system is open for improvement as was discussed in the design process. The PCB is designed for improvement of the system. Possible improvements are variable frequency control at the primary side. This solves the problem of a varying load for the battery charging application. Another improvement is the design of the coils. In the coil design, design guidelines are given for an optimal design for the system. Optimizing the coils affect the parameters of the compensation and the operating frequency, therefore the frequency will be adjustable on the PCB of the inverter.

A

Compensation parameters

(a) Reflected resistance & reactance		
Series Secondary	$\mathrm{Re}\,Z_{r0} = \frac{\omega_0^2 M^2}{R}$	$\mathrm{Im}\,Z_{r0} = 0$
Parallel Secondary	$\mathrm{Re}\,Z_{r0} = \frac{M^2 R}{L_s^2}$	$\mathrm{Im}\,Z_{r0} = -\frac{\omega_0 M^2}{L_s}$
(b) Primary capacitance		
SS Topology	$C_p = \frac{1}{\omega_0^2 L_p}$	
SP Topology	$C_p = \frac{1}{\omega_0^2 \left(L_p - M^2/L_s\right)}$	
PP Topology	$C_p = \frac{L_p - M^2/L_s}{\left(\frac{M^2 R}{L_s^2}\right)^2 + \omega_0^2 \left(L_p - M^2/L_s\right)^2}$	
PS Topology	$C_p = \frac{L_p}{\left(\frac{\omega_0^2 M^2}{R}\right)^2 + \omega_0^2 L_p^2}$	
(c) Primary & secondary quality factors		
Series Secondary	$Q_p = \frac{L_p R}{\omega_0 M^2}$	$Q_s = \frac{\omega_0 L_s}{R}$
Parallel Secondary	$Q_p = \frac{\omega_0 L_p L_s^2}{M^2 R}$	$Q_s = \frac{R}{\omega_0 L_s}$

Figure A.1: parameters of compensation topologies [33]

B

Inverter

B.1. Inverter components

Component	Value	Comments	Availability/Ordercode
R_{OVP1}	20K		
R_{OVP2}	46K		
R_{UVLO1}	20K		
R_{UVLO2}	172K		
RT	100K		
C_{VCC}	10 μF		
C	0.1 μF		
R_{CS}	0.3		
R_{filter}	1.1 K		
C_{filter}	15 nF		
C_{BST}	0.1 μF		
NMOS	NA	IPB530N15N3	Available at the Tellegen Hall
IC Adapter	NA	LCQT-TSSOP28	Farnell: 2476044
LM5045	NA		Farnell: 2064692

Table B.1: Inverter component overview

The components without a specified availability are available in the Tellegen Hall. Also, ceramic capacitors are preferred because of the low ESR.

B.2. Inverter schematic

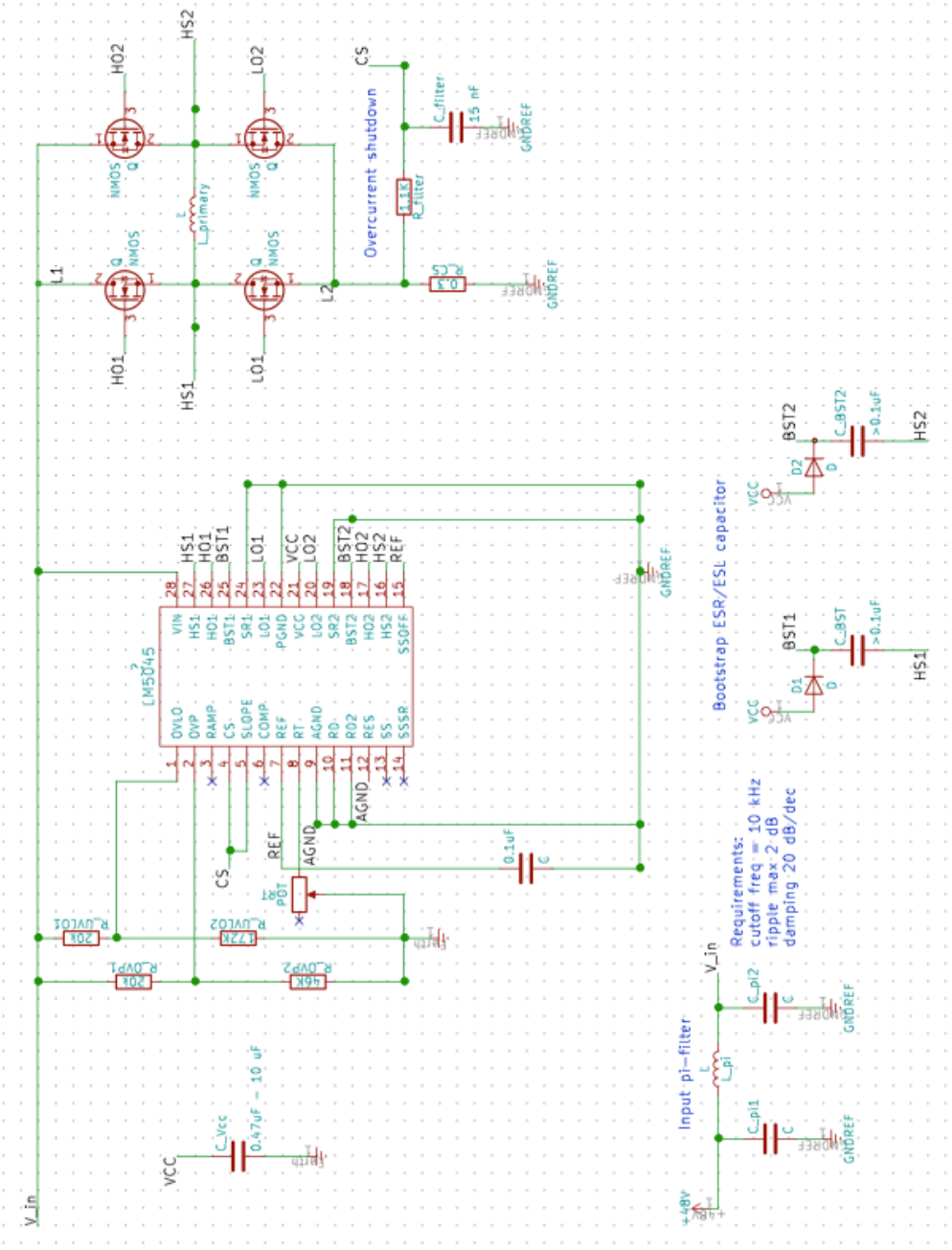

Figure B.1: KICAD schematic of the inverter design

C

Rectifier simulations

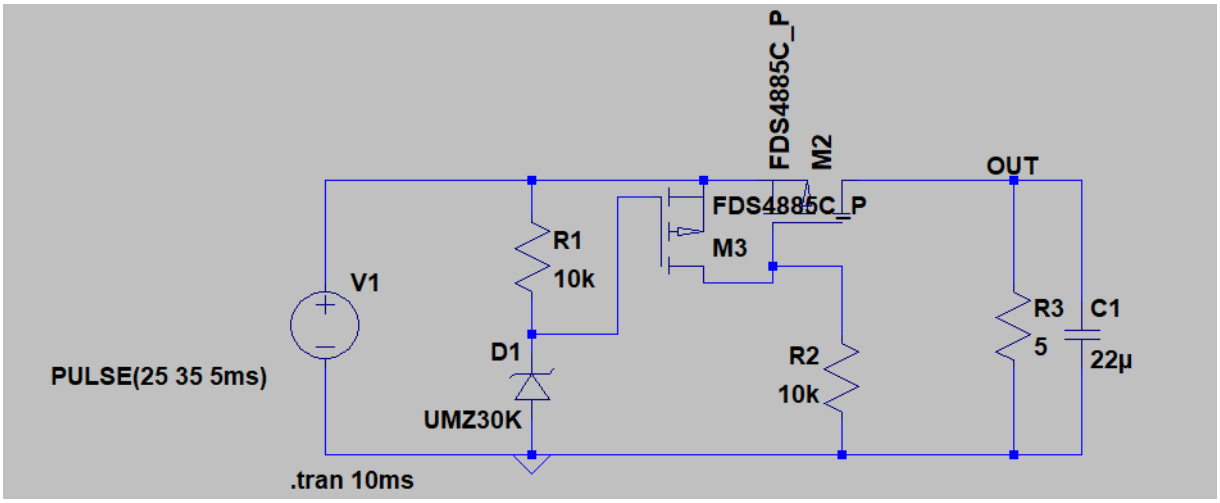

Figure C.1: Design of Over-voltage circuit

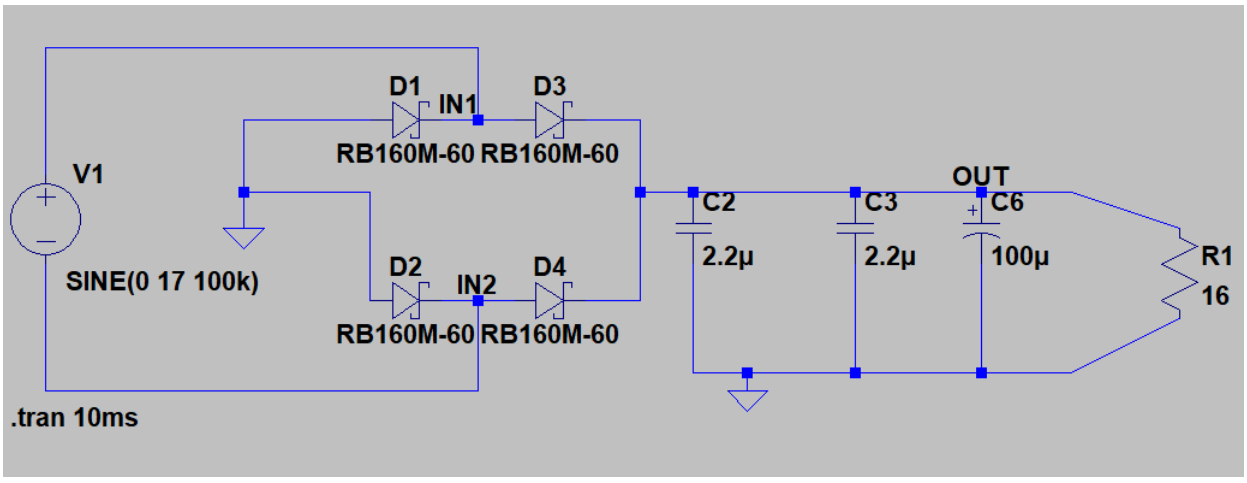

Figure C.2: Design of diode bridge with smoothing

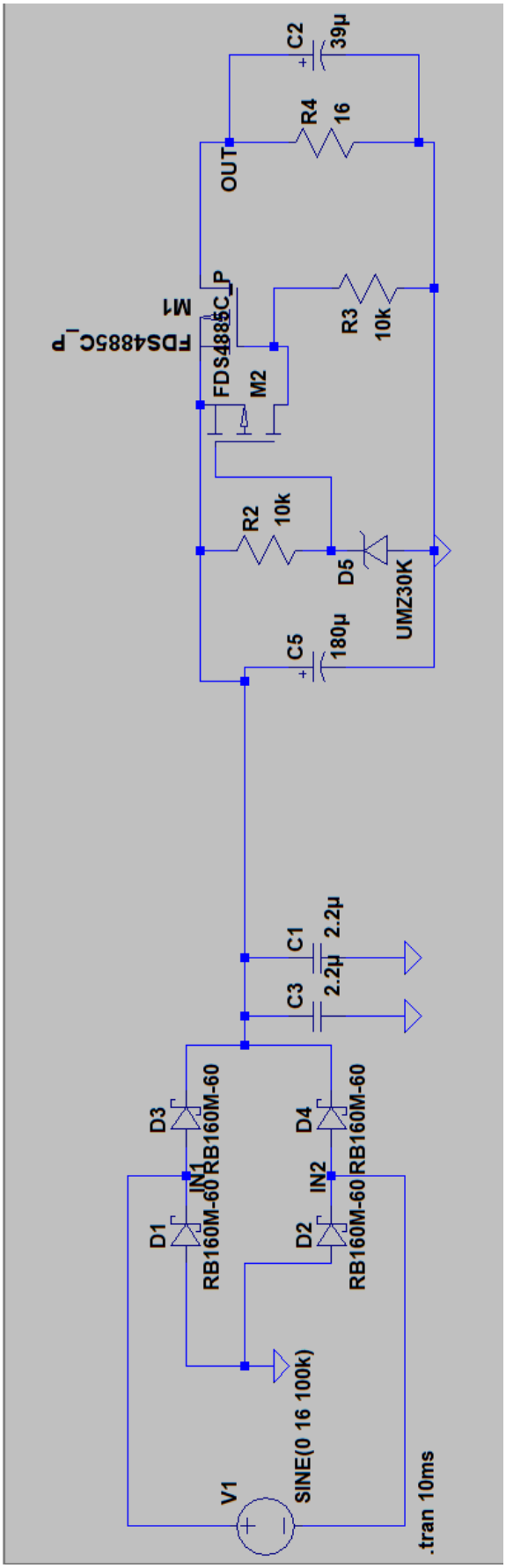

Figure C.3: Design of the whole rectifier, diode bridge with overvoltage protection

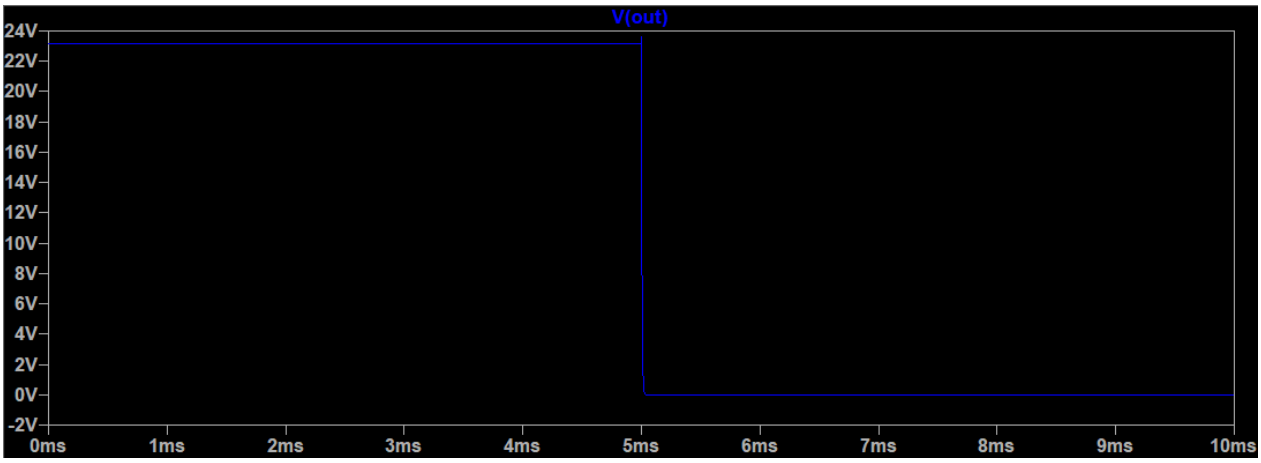

Figure C.4: Simulation of overvoltage circuit, input:25V after 5ms 35V

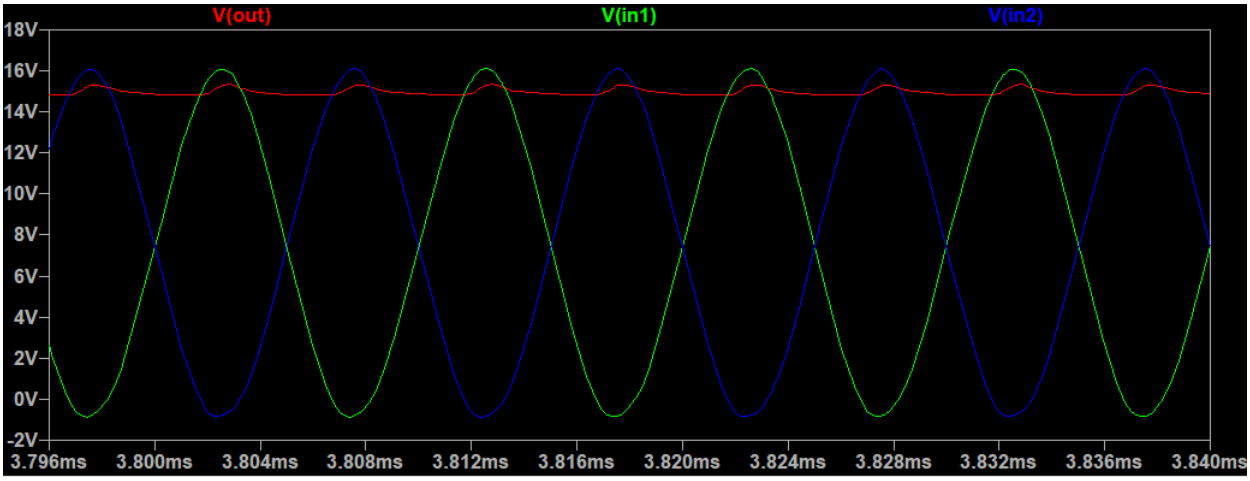

Figure C.5: Simulation of diode bridge with smoothing capacitance, input: 16V 100kHz

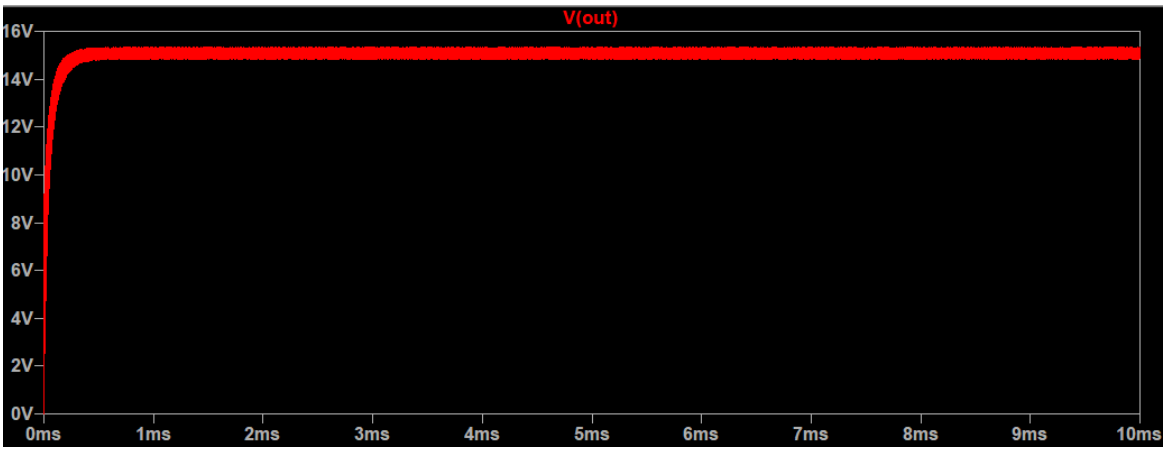

Figure C.6: output of diode bridge with smoothing capacitance, input: 16V 100kHz

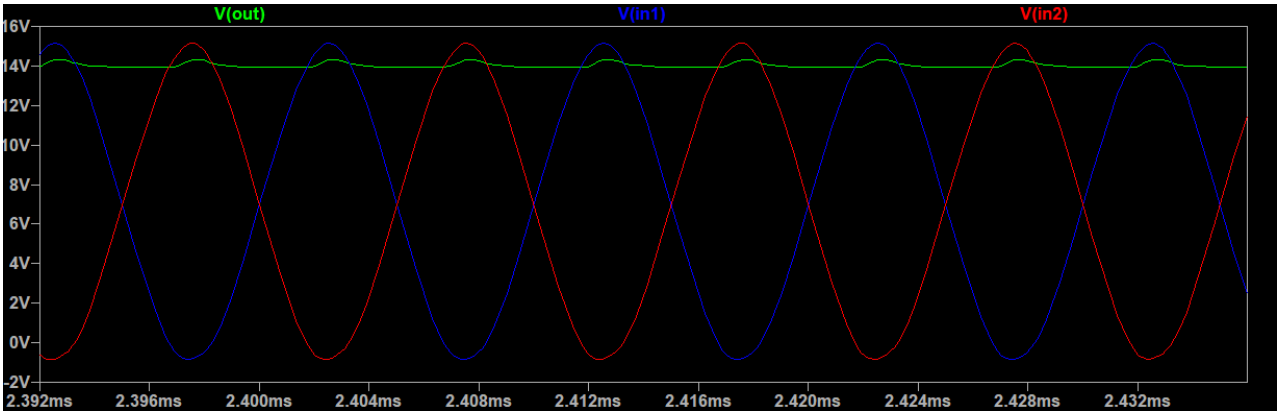

Figure C.7: The complete rectifier simulation: input:16V 100kHz

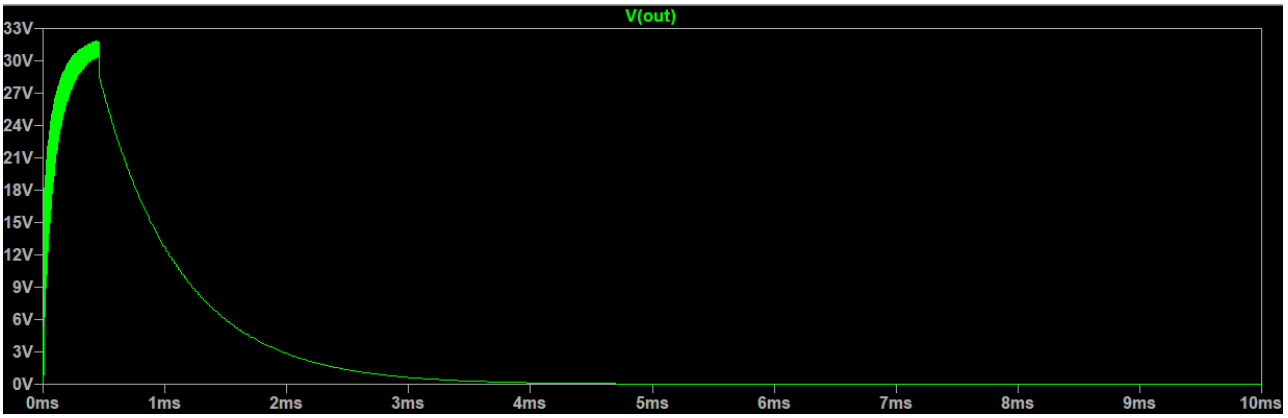

Figure C.8: The complete rectifier simulation: input:35V 100kHz

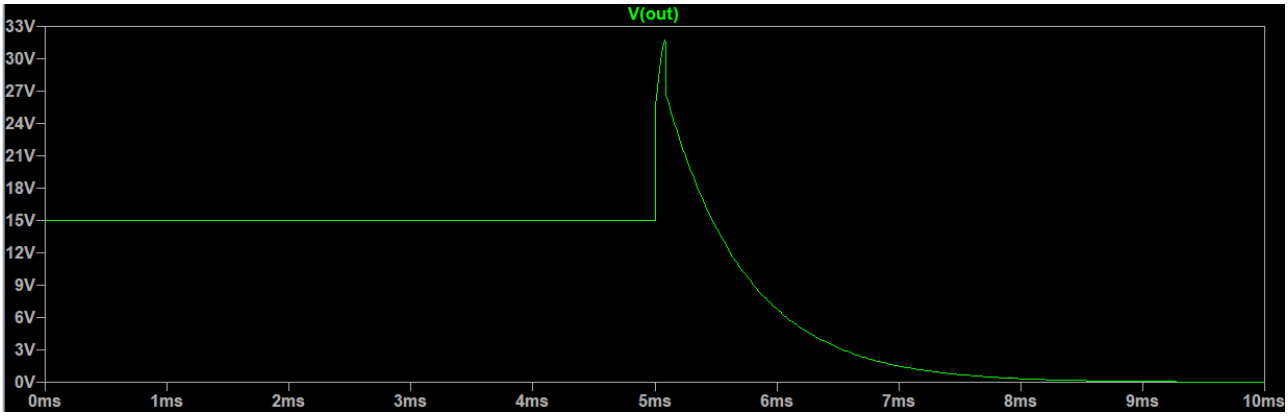

Figure C.9: The complete rectifier simulation: input:16V after 5ms 35V

D

PSPICE simulation

In this section the coupling factor is analyzed with respect to the operating frequency of the WPT system. The values of the coils and capacitors in the Design section chapter 4 are used for this analysis.

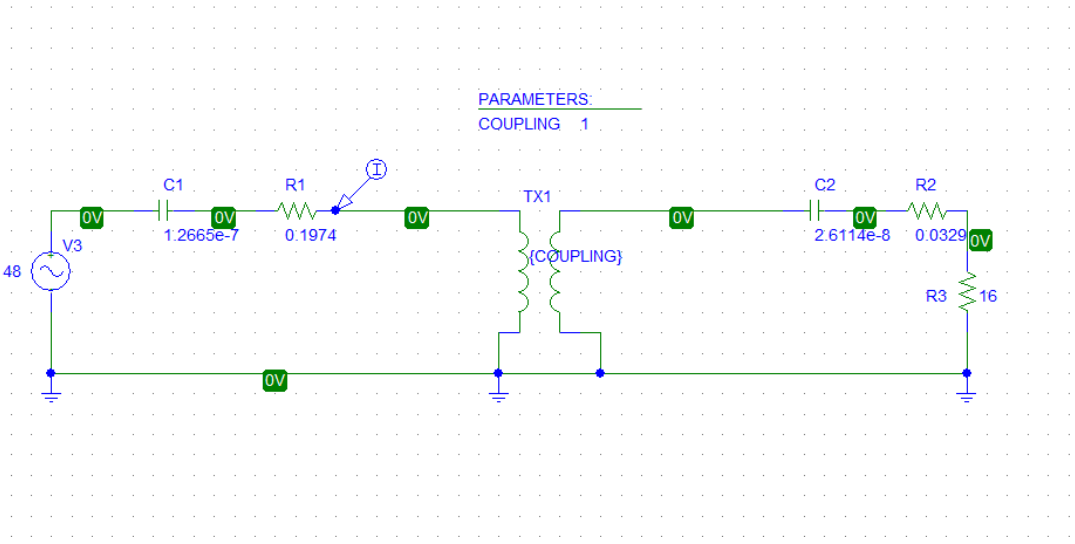

Figure D.1: Pspice simulation with varying coupling factor.

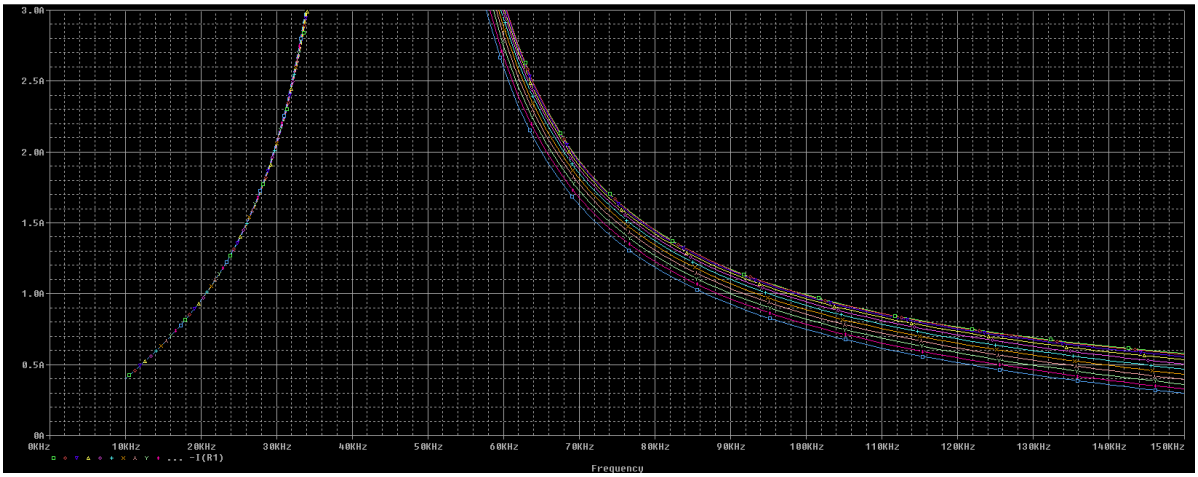

Figure D.2: The current through the primary coil vs the frequency with a varying coupling factor.

When varying the coupling factor in PSPICE the curve plotted in fig. D.2 can be extracted. The current through the primary coil versus the operating frequency is displayed in the graph. From this is it can be concluded that the frequency should be $> 60kHz$ such that the system won't exceed the current limit. The green line is for a coupling factor of zero ($k = 0$) and the blue line is for a perfect coupling of one ($k = 1$). The maximum coupling that could be achieved was a coupling factor of $k = 0.7$ Choosing an operating frequency depends on considering the maximum primary current and the efficiency of the whole system and other requirements of the system. For the design in this thesis an optimum was chosen at 100 kHz.

Bibliography

[1] K. Siddabattula, Why not a wire? the case for wireless power. .

[2] Icnirp statement on the "guidelines for limiting exposure to time-varying electric, magnetic, and electromagnetic fields (up to 300 ghz)", Health Physics 97, 257–258 (2009).

[3] R. Shadid, S. Noghanian, and A. Nejadpak, A literature survey of wireless power transfer, in 2016 IEEE International Conference on Electro Information Technology (EIT) (2016) pp. 0782–0787.

[4] J. Dai and D. C. Ludois, A survey of wireless power transfer and a critical comparison of inductive and capacitive coupling for small gap applications, IEEE Transactions on Power Electronics 30, 6017 (2015).

[5] K. v. Schuylenbergh and R. Puers, Inductive powering: basic theory and application to biomedical systems (Springer, 2009).

[6] C. K. Alexander and M. N. O. Sadiku, Fundamentals of electric circuits (McGraw-hill Education, 2017).

[7] B. Ferreira and W. V. d. Merwe, The Principles of Electronic and Electromechanic Power Conversion: A Systems Approach (John Wiley Sons, Inc, 2014).

[8] F. T. Ulaby and U. Ravaioli, Fundamentals of applied electromagnetics (Pearson Education Limited, 2015).

[9] W. Hurley and M. Duffy, Calculation of self and mutual impedances in planar magnetic structures, IEEE Transactions on Magnetics 31, 2416–2422 (1995).

[10] M. Q. Nguyen, P. Woods, Z. Hughes, Y. S. Seo, S. Rao, and J. C. Chiao, A mutual inductance approach for optimization of wireless energy transmission, in Texas Symposium on Wireless and Microwave Circuits and Systems (2014) pp. 1–4.

[11] N. Jamal, S. Saat, and A. Z. Shukor, A study on performances of different compensation topologies for loosely coupled inductive power transfer system, 2013 IEEE International Conference on Control System, Computing and Engineering (2013), 10.1109/iccsce.2013.6719954.

[12] O. Stielau and G. Covic, Design of loosely coupled inductive power transfer systems, PowerCon 2000. 2000 International Conference on Power System Technology. Proceedings (Cat. No.00EX409) 10.1109/icpst.2000.900036.

[13] Y.-H. Chao, J.-J. Shieh, C.-T. Pan, W.-C. Shen, and M.-P. Chen, A primary-side control strategy for series-parallel loosely coupled inductive power transfer systems, 2007 2nd IEEE Conference on Industrial Electronics and Applications (2007), 10.1109/iciea.2007.4318825.

[14] C.-S. Wang, G. A. Covic, and O. H. Stielau, Power transfer capability and bifurcation phenomena of loosely coupled inductive power transfer systems, IEEE Transactions on Industrial Electronics 51, 148 (2004).

[15] S. Chopra and P. Bauer, Analysis and design considerations for a contactless power transfer system, in 2011 IEEE 33rd International Telecommunications Energy Conference (INTELEC) (2011) pp. 1–6.

[16] C.-S. Wang, O. H. Stielau, and G. A. Covic, Design considerations for a contactless electric vehicle battery charger, IEEE Transactions on Industrial Electronics 52, 1308 (2005).

[17] L. R. Clare, S. G. Burrow, B. H. Stark, N. J. Grabham, and S. P. Beeby, Design of an inductive power transfer system with flexible coils for body-worn applications, Journal of Physics: Conference Series 660, 012135 (2015).

[18] Y. Gao, Frequency control, modeling, alignment adaptation, and safety concerns for the wireless charging of electric vehicles, Ph.D. thesis, University of Georgia.

[19] N. Liu, Design of a universal inductive charging system for electrical vehicles, Ph.D. thesis, Georgia Institute of Technology.

[20] www.wirelesspowerconsortium.com, .

[21] http://www.airfuel.org, .

[22] The future of wireless power standards: Qi vs. rezence, .

[23] LM5045 Full-Bridge PWM Controller With Integrated MOSFET Drivers, Texas Instruments (2015), rev. H.

[24] J. Adams, Application note an-1052 - international rectifier, (2003).

[25] A. Prakash, Current Sensing in an H-Bridge, Texas Instruments (2016).

[26] R. Bosshard, J. Mühlethaler, J. W. Kolar, and I. Stevanović, Optimized magnetic design for inductive power transfer coils, in 2013 Twenty-Eighth Annual IEEE Applied Power Electronics Conference and Exposition (APEC) (2013) pp. 1812–1819.

[27] J. Garnica, R. A. Chinga, and J. Lin, Wireless power transmission: From far field to near field, Proceedings of the IEEE 101, 1321 (2013).

[28] J.-R. Riba, Calculation of the ac to dc resistance ratio of conductive nonmagnetic straight conductors by applying fem simulations, European Journal of Physics 36, 055019 (2015).

[29] K. Wu, Introduction To SCHOTTKY Rectifier and Application Guidelines, Taiwan Semiconductor.

[30] Silicon Carbide Schottky Diodes:Novel devices require novel design rules, Infineon Technologies Austria AG.

[31] Electronics-tutorials, Full wave rectifier, (2017).

[32] IRF9530, SiHF9530:Power MOSFET, Vishay Siliconix (2016), rev. C.

[33] C.-S. Wang, G. Covic, and O. Stielau, Power transfer capability and bifurcation phenomena of loosely coupled inductive power transfer systems, IEEE Transactions on Industrial Electronics 51, 148–157 (2004).